Time-Resolved X-Ray Absorption Spectroscopy (XAS)

28

Bert M. Weckhuysen , Caterina Suzanna Wondergem , and Charlotte Vogt

Contents

Abstract

X-ray absorption spectroscopy (XAS) plays a crucial role in the characterization of catalysts as it can in principle characterize any chemical element under well-defined conditions (i.e., in the liquid, gas, and solid phase) as well as under reaction conditions (i.e., at elevated temperatures and pressures, in the so-called *in situ* or *operando* mode). The past decades have seen an increase in XAS capabilities in part due to the higher brilliance of X-ray sources at synchrotrons, which in combination with more powerful detectors and optics allows to conduct time-resolved measurements, such as sub-second X-ray absorption near-edge spectroscopy (XANES). Such measurements allow investigation of solid catalysts at different stages of existence, i.e., their birth, life, and death. Furthermore, by the combination of XANES with microscopic capabilities by use of Fresnel zone plates to focus, X-rays allow for 2D and 3D imaging of a catalyst material as a function of reaction time, while the further development of lab-based X-ray source has made it possible to bring the X-ray experiment into both academic and industrial labs, comparable to what we currently do for measuring, e.g., X-ray diffraction (XRD) and Raman spectroscopy. Finally, as no single analytical technique can offer the ultimate answer to a scientific question, often (time-resolved) XAS is combined with optical, diffraction, and/or scattering methods, thereby allowing to distinguish between local and structural (bulk) properties of catalyst materials. The above-described developments will be illustrated by using a selection of showcases. The chapter concludes with some general observations as well as with an outlook.

B. M. Weckhuysen (✉)
Inorganic Chemistry and Catalysis, Debye Institute for Nanomaterials Science, Utrecht University, CG Utrecht, The Netherlands
e-mail: b.m.weckhuysen@uu.nl

C. S. Wondergem
Research Center for Materials Science, Graduate School of Science, Nagoya University, Nagoya, Japan
e-mail: cswondergem@chem.nagoya-u.ac.jp

C. Vogt
Schulich Faculty of Chemistry, Technion, Israel Institute of Technology, Haifa, Israel
e-mail: c.vogt@technion.ac.il

28.1   Basic Concepts of X-Ray Spectroscopy

28.1.1   Interaction of X-Rays with Matter

Electromagnetic radiation interacts with matter in ways that are characteristic for the type of matter, depending on the energy of the light. X-rays are generally defined as photons with energies between 0.1 keV and 200 keV (approximately 6 pm–12 nm, Fig. 28.1a). Such photons have the ability to interact with electrons that surround the cores of atoms, namely, core electrons [1–5]. Unlike valence electrons, which make up the outer shells of an atom, core electrons are tightly bound to the nucleus and do not participate in chemical bonding. Because of their tight binding to the nucleus, the energy required to excite them to an unoccupied orbital is relatively high. The closer the electrons are located to the positively charged core, the higher this energy requirement becomes [6]. The core electron shells are termed K, L, M, and N, depending on their vicinity to the core (Fig. 28.1b). Their nomenclature is based on quantum numbers, i.e., 1s corresponds to K, 2s and 2p to L, and so on. This means that within one element, electrons in the K shell require the highest amount of energy for excitation as this corresponds to the excitation of a 1s electron. The energy at which the excitation of a 1s electron occurs is called the "K-edge" (>1 keV for transition metals). The required energy for excitation decreases moving to the L- and M-edges (generally ~0.1–1 keV for (transition) metals) [7]. This is illustrated in Fig. 28.1c, where the absorption edges of the K, L, and M shells and their corresponding orbitals are shown as a function of energy. X-ray absorption spectroscopy (XAS) is used to measure these edge energies and to analyze the properties of the core electrons of an element under investigation. XAS is a bulk technique, and as such the spectrum that results from the acquired XAS data is that of the average atom in the sample.

To obtain an X-ray absorption spectrum, the sample under study is exposed to an X-ray source, which scans along a range of relevant energies close to a known absorption edge of the element under study [6, 7]. An intensity jump in the spectrum can be observed at a specific energy, which relates to the absorption of photons by the sample as a function of energy. Three distinct energy-dependent events are of importance while scanning X-rays across an absorption edge. These three events give rise to distinct features in X-ray absorption spectra [2, 5]:

1. The pre-edge, the threshold of absorption which is distinct for excitations into the lowest unoccupied states.
2. The edge, where core transitions to quasi-bound states occur.
3. Scattering of electrons with neighboring atoms. In the high-kinetic-energy range, the constructive and destructive interference of the resonance of excited electrons at fixed positions of neighboring atoms gives rise to clearly distinguishable absorption features (oscillations).

A typical example of an X-ray absorption spectrum featuring the abovementioned events is shown in Fig. 28.1d, including the division of the spectrum in two separate regions. These two regions are referred to as the X-ray absorption near-edge structure (XANES), also known as near-edge X-ray absorption fine structure (NEXAFS), and the extended X-ray absorption fine structure (EXAFS). In XANES, events 1 and 2 can be observed. This technique focuses on the absorption edge, approximately 200 eV before the edge and approximately 1000 eV after it for K-edge spectra of transition metals. The scattering of electrons with neighboring atoms, event 3, is what is considered in EXAFS, which is found in the higher-kinetic-energy region of the X-ray absorption spectra [5–7].

The areas of a spectrum corresponding to these separate events hold different information on the material under study. First, the energy of the measured edge gives information on the characteristic absorption edge of the material and thus yields element-specific information [8]. For the K-edge, this involves excitation from the 1s ➔ p shells. Since there is only one electron in an s-orbital, there is only one (main) K-edge. There are however three L-edges, since these involve both an s and two p-orbitals. The L_1-edge corresponds to s ➔ p transitions, while the L_2- and L_3-edges correspond to p ➔ d transitions. The former is excited at higher energy than the latter two, which generally occur closer to each other in energy (Fig. 28.1c), and can even overlap or be difficult to distinguish in a spectrum. This also complicates the scattering spectrum in the high-kinetic-energy range, requiring different modes of measurement. These different edges not only give information on which element is being studied, but also provide information on the average oxidation state.

When observing the profile of a K-edge spectrum in more detail, often a small peak can be observed in the lower-energy region of the spectrum, right before the intense increase in absorption. This is the pre-edge (point 1 described above), corresponding to the excitation of a 1s electron to an unoccupied d-orbital (this is a dipole-forbidden, quadrupole-allowed transition and therefore a much weaker feature than the electric dipole allowed 1s to p-orbital transitions). This pre-edge can already give information on the oxidation state of the average atom by revealing the occupancy of the d-orbitals [2, 9]. This includes the observation of ligand (geometry) and local distortions, e.g., Chen *et al.* reported strong geometry-dependent 3d molecular orbital energies, resulting in a broad 1s ➔ $3d_{x2-y2}$ transition and elongated M-R bonds in their studies of
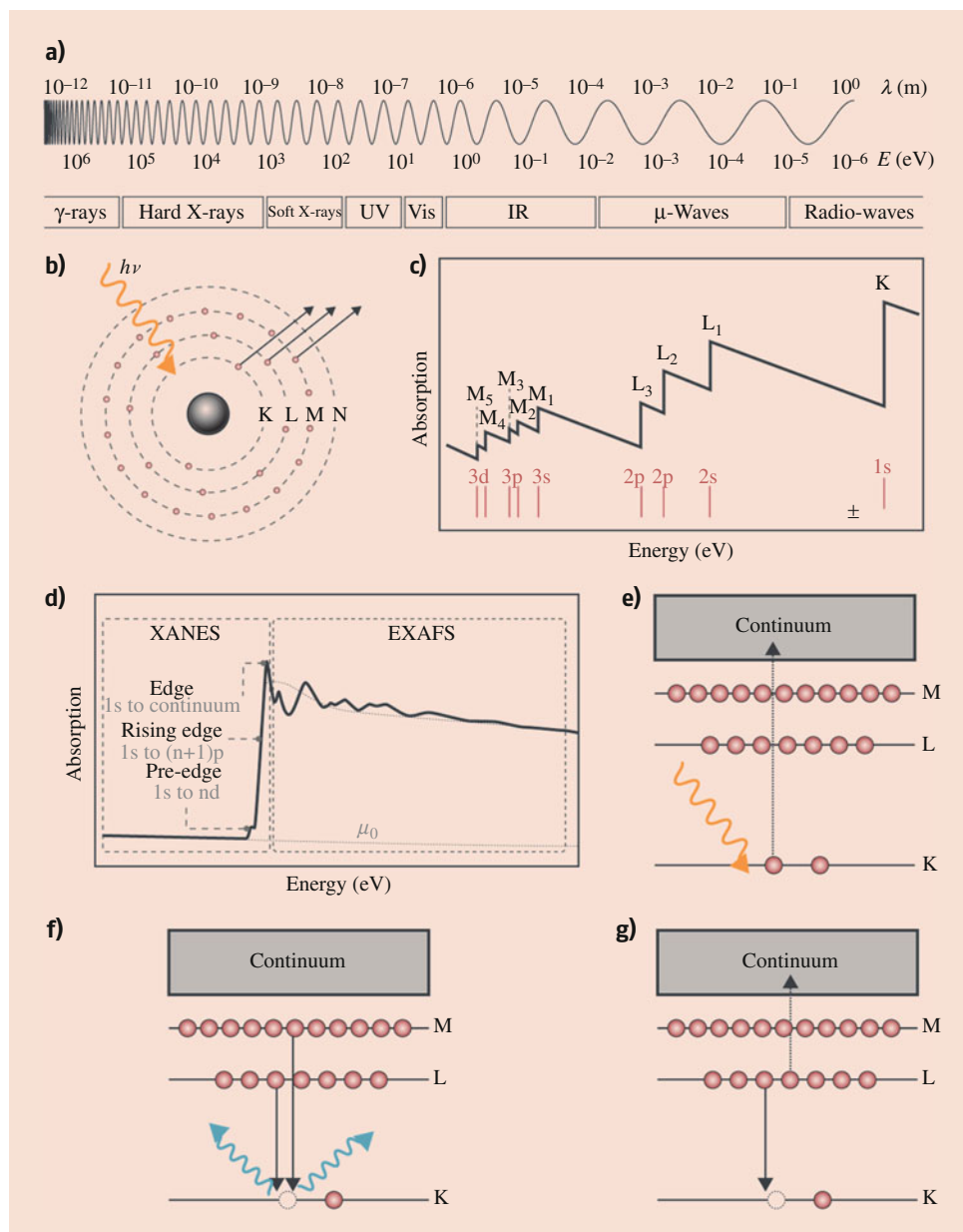
Fig. 28.1 (**a**) Wavelengths in m (upper number) and corresponding energies in eV (lower numbers) of electromagnetic radiation or light. The electromagnetic radiation can be divided into subgroups as indicated in the figure. X-rays constitute the range of 0.1–200 keV and in turn can be divided into hard and soft X-rays, where the first has higher energy than the latter; (**b**) schematic representation of core electron excitation from the K, L, and M shell by incoming light with sufficient energy (i.e., X-rays); (**c**) schematic representation of absorption edges. The highest energy is required to excite a core electron from the 1s or K shell, followed by the L (2s, 2p) and M (3s, 3p, 3d) shells; (**d**) typical example of an X-ray absorption spectrum, depicting the X-ray absorption near-edge structure (XANES) and the extended X-ray absorption fine structure (EXAFS); (**e**) schematic representation of X-ray absorption, where an incident X-ray photon excites a core electron, ejecting it from the atom (into the continuum). The excited atom can fill the core hole through several mechanisms to return to the ground state; (**f**) schematic representation of X-ray fluorescence. Electrons from higher shells (i.e., for K shell core holes, electrons from the L and M shells) fill the core hole, releasing X-ray photons with characteristic energies depending on the element and shell; (**g**) schematic representation of Auger electron emission. The core hole is filled by an electron from a higher shell, while emitting an electron of the same shell into the continuum

axial ligation of Ni metalloporphyrins [10, 11]. As mentioned, the pre-edge and the edge together are often referred to as the XANES or NEXAFS regions. The XANES region of an X-ray absorption spectrum is generally used to determine electronic (e.g., oxidation state) and (to a lesser extent) geometric information about the sample. Examples are estimations of ligand fields, spin states, or the charge on a metal carrier (oxidation state).

Above the edge, at high kinetic energies, we can observe the EXAFS as post-edge oscillations [5, 12]. These oscillations originate from scattering interactions of the emitted electrons with neighboring atoms. The resulting constructive and destructive interference results in the oscillations observed in the EXAFS and thereby provides information on the local surroundings of an atom [13]. The EXAFS is generally used to determine precise local *geometric* information on the average absorbing atom. First, the spacing between the oscillations or their frequency is inversely proportional to the distance between the atom that absorbed the X-ray photon and a neighboring atom that the emitted electron scattered off of, allowing determination of the average local atomic surroundings. For example, if a solid being measured is in its metallic form, the distance between two atoms will be larger than when the solid is oxidized. In the latter case, the scattering atoms (oxygen) would be found at a position that is closer to the atom than a metallic neighbor would be (i.e., at bond lengths of below 2 Å, whereas metal-metal bonds are found at around or above 2 Å).

Additionally, scattering probability generally increases with atomic mass and is element-dependent, meaning that we can extract information not only about the distance to neighboring atoms but also about their nature. Finally, the amplitude of the EXAFS oscillations reflects the number of scattering neighbors and thus can be used as a measure for the average coordination number of the element under study.

If the element of interest is present in low concentrations, insufficient signal might be obtained following XAS measurement configuration. In this case, X-ray emission spectroscopy, XES, techniques may be employed to collect spectra with good signal-to-noise ratios [2, 6, 7].

XES is closely related and complementary to XAS. Figure 28.1e illustrates how a core hole is created upon X-ray absorption. This core hole can be filled by an electron from a higher shell through the mechanisms shown in Fig. 28.1f, g. The emitted photons or electrons can be detected, leading to X-ray fluorescence spectroscopy (XRF) and Auger electron spectroscopy, respectively.

28.1.2 The EXAFS Equation

The description given so far has been purely qualitative, but it *can* be derived using quantum mechanics. This derivation results in what is often referred to as the EXAFS equation in which the EXAFS signal $\chi(k)$ is expressed as the sum of the different contributions. Note first that the EXAFS equation is given as a function of k, wave number, and not of E, energy, by the following conversion:

$$k = 1/\hbar\sqrt{(2m_e(E-E_0))},$$

and with that:

$$\chi(k) = S_0^2 \Sigma(N_i) {}_f(k)/kD_i^{2*} e^{-2D/\lambda(k)*} e^{-2k^2\sigma^2} \sin(2kD_i + \delta_i(k)),$$

where S_0^2 represents the amplitude reduction factor, which is an element-dependent (and sample-specific) constant that accounts for the increased influence that the electrons experience from the positively charged nucleus after the emission of a core electron. This results in the orbitals adapting to the decrease in shielding from the core, or in other words, it results in relaxation of all the other electrons in the absorbing atom. Because there is now a slight symmetry mismatch in orbitals compared to the initial atom, the amplitude of EXAFS oscillations is reduced by a factor of S_0^2. This term is obtained for EXAFS analysis by measuring a standard for the specific experimental or beamline setup and generally lies (or is kept) between 0.7 and 1.0.

N_i in the EXAFS equation represents the degeneracy, or the number of neighbors of the absorbing atom. Upon inspection of the expression for the EXAFS absorption as a function of the wave number, $\chi(k)$, we see that if we know $f_i(k)$ and $\delta_i(k)$ we can determine the coordination number of the neighboring atom. $f_i(k)$ and $\delta_i(k)$ are both dependent on atomic number and represent the scattering amplitude and the phase shift, respectively. These factors can be calculated, given a valid approximation of the periodic structure of the sample, by software that was built to model EXAFS.

Aside from the degeneracy N_i, the EXAFS equation can also be used to determine D_i (the distance from the absorber to the scatterer and back, often represented a R) and σ, the measure of disorder in neighboring atoms. These factors are the quantitative descriptors to what was described in the last paragraph of the previous section.

As the EXAFS equation implies, data is often represented in k-space to show dependence of momentum instead of energy. Additionally, data can be weighted (often by k^2 or k^3) to reveal weak signals at high kinetic energies, even though this approach generally also amplifies noise. Subsequently, the EXAFS data in the form of (k-weighted) $\chi(k)$ will often undergo a Fourier transform, resulting in the expression of χ in R-space, which is related to a radial distribution function. This can in turn be fitted using specialized EXAFS software to obtain information on bond distances. However, the trained eye can already gain preliminary understanding based on distinguishable features.

Ultimately, proper analysis of XAS results cannot be performed without the measurement of appropriate standards and reference materials. This requires some level of understanding of the system under study – often obtained through standard laboratory techniques – before conducting X-ray experiments. For example, transmission electron microscopy can be used to determine nanoparticle size and dispersion, and when combined with energy-dispersive X-ray spectroscopy, the correct edges to consider can be determined; UV-Vis spectroscopy can be used to get an idea of charge

transfer mechanisms, and probe molecule (infrared) spectroscopy can reveal the type of sites present in a sample. This knowledge should be used to determine appropriate standards. Along with possible modeling and calculation of EXAFS using dedicated software (e.g., Artemis, Larch), such appropriate standards are essential to a successful XAS experiment and its in-depth analysis. For more information on data treatment and dedicated EXAFS software, we refer the reader to a number of textbooks [2, 5–7].

28.2   The X-Ray Absorption Experiment

28.2.1   The X-Ray Source

Synchrotron Radiation Sources
Because a range of energies at high photon flux in the X-ray energy range is required to measure XAS data, standard laboratory equipment could not be used for a long time. Instead, a tunable X-ray source is employed, often in the form of a synchrotron or particle accelerator, which produces light in a broad range of wavelengths and with a high photon flux by the circulation of electrons in a storage ring [14]. A

schematic overview of a synchrotron and its workings is given in Fig. 28.2. After generation of electrons in an electron gun, they are accelerated to (nearly) the speed of light in a linear accelerator. They are then transferred to the booster ring, with the aim of increasing their energy to the desired level. This level differs per synchrotron radiation facility. For example, the Super Photon Ring-8 (SPring-8) in Japan operates at 8 GeV, while the Swiss Light Source (SLS) in Switzerland operates at 2.4 GeV, and the Advanced Light Source (ALS) in the United States operates at 1.9 GeV. Finally, the electrons are moved to the storage ring, where they can be used to generate electromagnetic radiation with high photon flux [15]. The trajectory of the electrons in the storage ring is determined by bending magnets, steering them in a circle instead of a straight line. This comes with the release of energy, i.e., light, with a broad range of wavelengths and high photon flux. The generated light can be extracted from the storage ring in beamlines, which are placed at specific locations in the storage ring and as such can be used for experiments. Furthermore, beamlines can be built behind undulators and wigglers, which are different types of equipment in the storage ring that induce movement in the electrons and thus produce X-rays. Light generated at
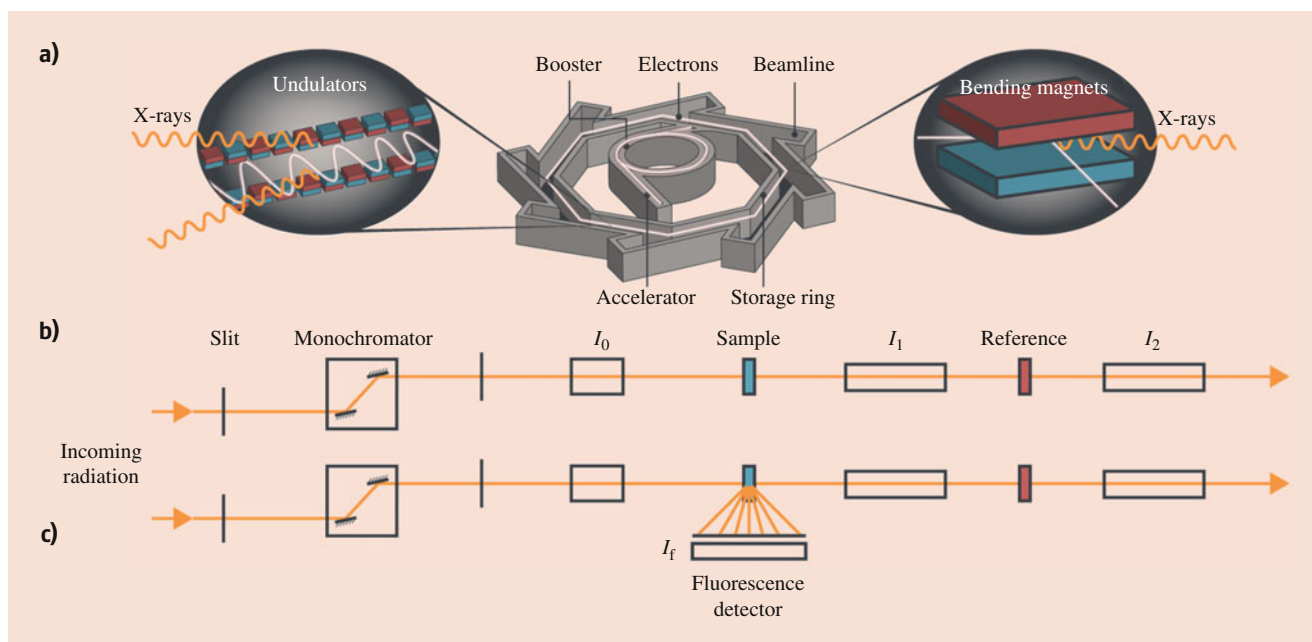

Fig. 28.2 (**a**) Schematic illustration of a synchrotron light source. After generation, electrons are accelerated to nearly the speed of light in the accelerator and when entering the booster ring undergo an increase in their energy to the desired level. They are then transferred to the storage ring where they pass by bending magnets and insertion devices (i.e., undulators and wigglers) to generate the desired X-ray beam. Bending magnets change the trajectory of the electron bunch, while insertion devices like undulators consist of magnets with alternating poles; (**b**) schematic setup of an X-ray absorption experiment. After extraction from the storage ring, the X-rays pass through a slit to tune the beam

size. Subsequently, a monochromator in combination with another slit is used to select the desired energy of the X-ray beam. The X-ray beam then passes through the first ionization chamber, I_0, which is a gas-filled radiation integration detector, before passing through the sample. After the sample, the beam passes through another ionization chamber, I_1. If a reference sample is measured alongside the sample, it will be placed after I_1, and another ionization chamber, I_2, will be employed; (**c**) X-ray fluorescence experiment. The setup is virtually the same as described in a, but a fluorescence detector (I_f) is placed at an angle θ with respect to the sample and usually contains more than one detection channel

bending magnets, undulators, and wigglers all have their own photon flux (with the latter two resulting in a more brilliant beam than bending magnets) and energy range which in turn all come with their own advantages and drawbacks.

Electrons travel together in small groups called bunches, and only when these bunches pass by the bending magnets, undulators, or wigglers, light is generated. The bunches are present in pulses in the GHz range, which means that for most practical purposes, the generated light can be deemed continuous [2, 7].

Lab-Based X-Ray Absorption Spectroscopy

Recently, lab-based X-ray spectroscopy methods have been developed that can meet the requirements for XAS, i.e., high photon flux over a range of X-ray energies. Lab-based X-ray sources generally comprise X-ray tubes, which are vacuum tubes consisting of a cathode and an anode side, as can be seen in Fig. 28.3. Electrons are generated at the cathode by applying a voltage, and X-rays are generated at the anode. Most of the energy is converted into heat; only about ~1% is converted into X-rays and can be used as light source for a spectroscopy experiment. To obtain sufficiently high photon flux, the voltage can be increased, but due to the high amount of heat generation, the melting point of the anode (often a metal like W) is a limiting factor of X-ray tubes. Therefore, with the aim of applying XAS in the lab, studies have focused on overcoming these limitations by implementing cooling techniques, alternative anode materials, and using techniques that lower the heat dissipation.

An example comprises rotation of the anode. As most of the heat is generated at the focal spot, which is typically very small, rotating the anode means a more homogeneous irradiation and thus lower average temperature generated. Alternatively, by focusing the electron beam as a line instead of a spot, heat dissipation becomes much more efficient. Such a source is called a line focus X-ray tube, LFXT, and is regarded a promising new development in the lab-based XAS community.

Apart from the developments in the X-ray source area of the setup, significant advances in detection equipment also contribute to the ongoing increase of implementation of lab-based XAS. Techniques like wavelength-dispersive X-ray (WDX) detection that originated at synchrotron beamlines can be used in a lab setup as well, increasing the energy resolution. WDX detectors exploit Bragg's law to achieve spatial dispersion of photons, and they can be used both for soft and hard X-ray experiments, although with slightly different setups.

The advances in lab-based XAS methodologies have made it possible to obtain spectra in the lab that are similar to those obtained at synchrotrons. This has been shown by, e.g., Moya-Cancino *et al.,* who demonstrate that despite a lower signal-to-noise ratio, the observed spectral features in their XAS spectra of the Co K-edge for a Co/TiO_2 Fischer-Tropsch synthesis (FTS) catalyst closely resemble spectra obtained on the same system measured at a synchr a synchrotron radiation facility, which can be seen in Fig. 28.3c [16]. For a more detailed and comprehensive overview of various lab-based setups and their development, we refer the interested reader to the excellent review article recently published by Zimmerman *et al.* [17] The authors expect that lab-based XAS will become more routine and eventually will be used in a similar manner as we are currently doing with lab-based X-ray diffraction (XRD).

Free Electron Lasers

XAS experiments can also be carried out at facilities where free electron lasers (FELs) are available [18, 19]. In FELs, electrons are accelerated close to the speed of light and led by a number of undulators, producing light through the same physical principles as in storage rings. Through interaction of the produced radiation with the oscillation of the electrons, micro-bunches producing coherent radiation are formed. This results in intense X-ray pulses that can be used for ultrahigh time resolution XAS experiments [20]. The emission wavelength of FELs is tunable by adjusting the magnetic field strength of the undulators. The authors expect that a lot of exciting new time-resolved studies will become feasible with FELs, especially where repetition-type experiments can be conducted. The latter is possible when studying photocatalytic processes.

Soft Versus Hard X-Rays

X-rays are roughly divided into two types: soft (i.e., below ~5 keV) and hard X-rays (i.e., above 5 keV), although the region between 2 and 5 keV is sometimes also referred to as tender X-rays. Hence, soft X-rays have lower energy than hard X-rays and interact to a greater extent with absorbing materials they come across. On the one hand, the lower amount of energy they carry makes it easier for them to interact with light materials, while on the other hand the attenuation length in heavy materials is much lower than that for hard X-rays. These two together potentially make the collection of sufficient signal challenging in soft X-ray experiments. In that sense, it seems preferable to use hard X-rays that have a larger penetration depth, but the drawback is that these cannot detect some light materials with absorption edges at relatively low energies, like carbon. Generally speaking, hard X-rays are often applied to measure transition metals. The main reasons for this are ease of use, or increased practicality in experimental setups, and better signal. For these reasons, spectral acquisition times can currently be as low as tens of milliseconds at especially equipped beamlines (i.e., quick-XAS, QXAS). The large majority of XAS beamlines comprises hard X-ray beamlines for measurement of transition metal-based catalysts. Figure 28.4 shows two reactor designs, one that is typically
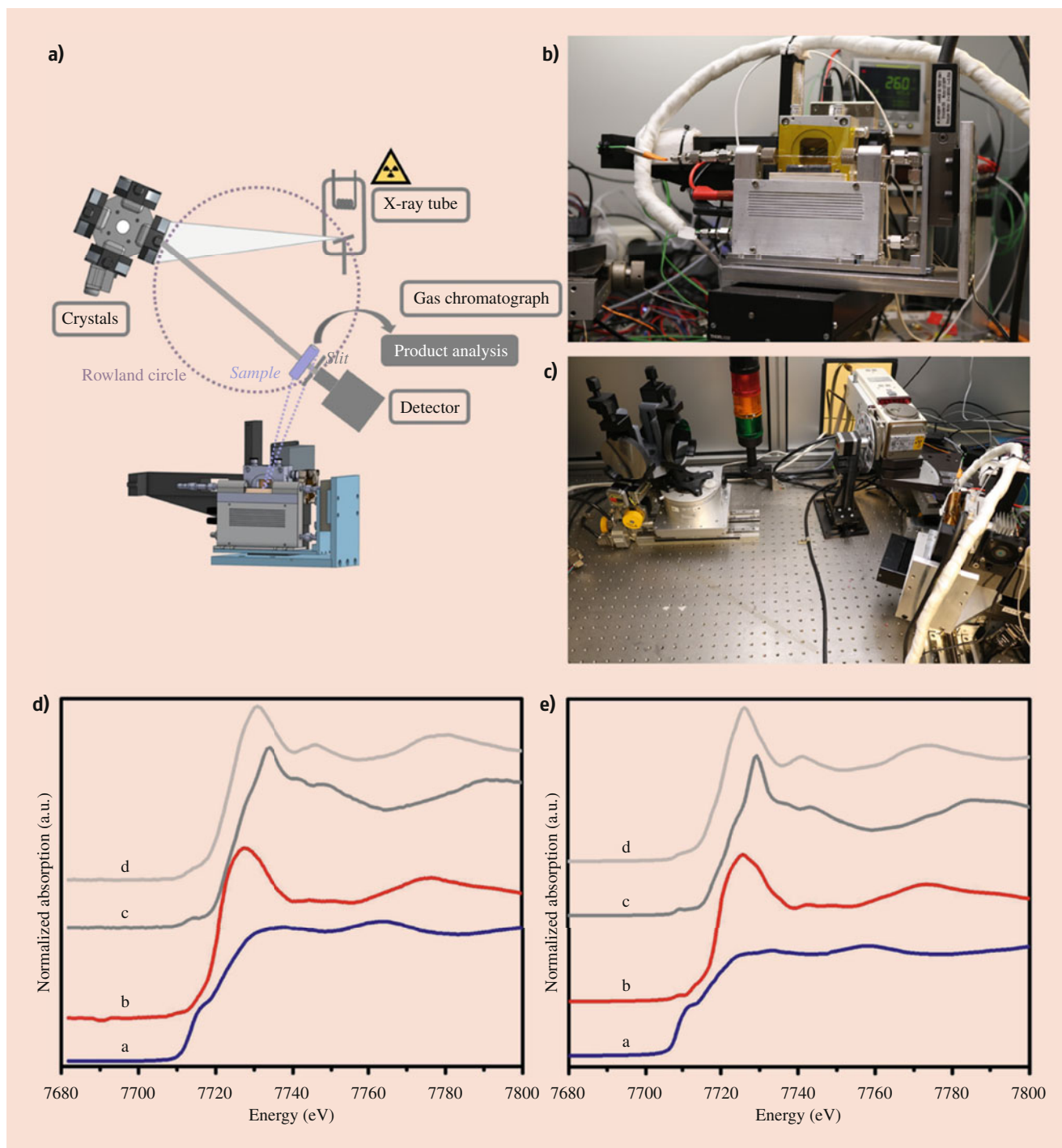
Fig. 28.3 (**a**) Schematic and (**b**, **c**) photographs of a lab-based X-ray absorption spectroscopy setup to perform time-resolved long-duration *operando* spectroscopy of solid catalysts. (**d**, **e**) Comparison between lab-based X-ray absorption spectra (**d**) and synchrotron-based X-ray absorption spectra (**e**) [64] for cobalt reference materials measured: (**a**) Co, (**b**) CoTiO$_3$, (**c**) Co$_3$O$_4$, and (**d**) CoO, thereby illustrating the overall quality of the performance of current lab-based setups. (Reproduced from [64], with permission from Wiley-VCH)

used for soft X-ray techniques called a micro-electromechanical system (MEMS) reactor. MEMS reactors can be used both for liquid and solid studies (provided that the attenuation length of the components to study does not lead to total absorption). The other is a capillary reactor that is – in different variations – often the choice for *operando* studies of heterogeneous catalyst powders reacting mainly with gases. It can be used, for example, in combination with hard X-ray microscopy and provides 3D information on, e.g., metals in a catalyst particle.
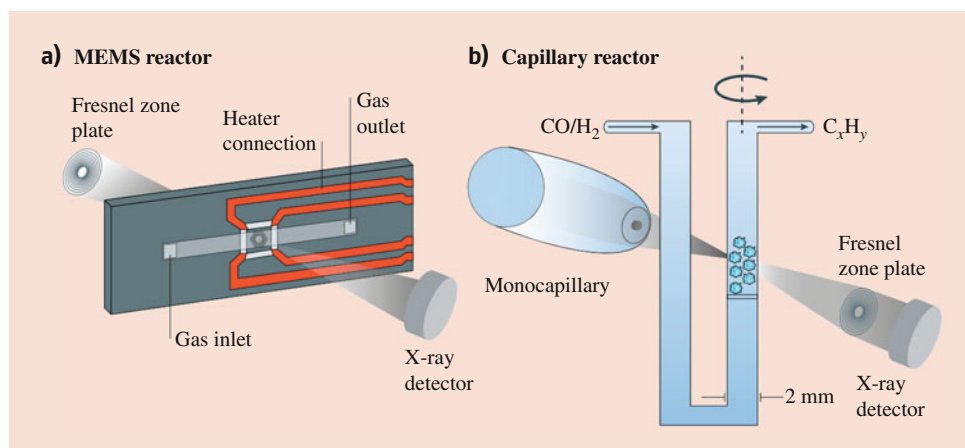
Fig. 28.4 (**a**) A microelectromechanical system (MEMS) reactor, which can be used for time-resolved long-duration *in situ* or *operando* soft X-ray spectroscopy experiments, as illustrated in Fig. 28.6. (**b**) A capillary reactor, which can be used for time-resolved long-duration *in situ* or *operando* hard X-ray absorption spectroscopy of solid catalysts, as illustrated in Fig. 28.7a. Both reactor designs have been used to study, for example, the Fischer-Tropsch synthesis (FTS) reaction over a Co/TiO$_2$ catalyst system under realistic reaction conditions
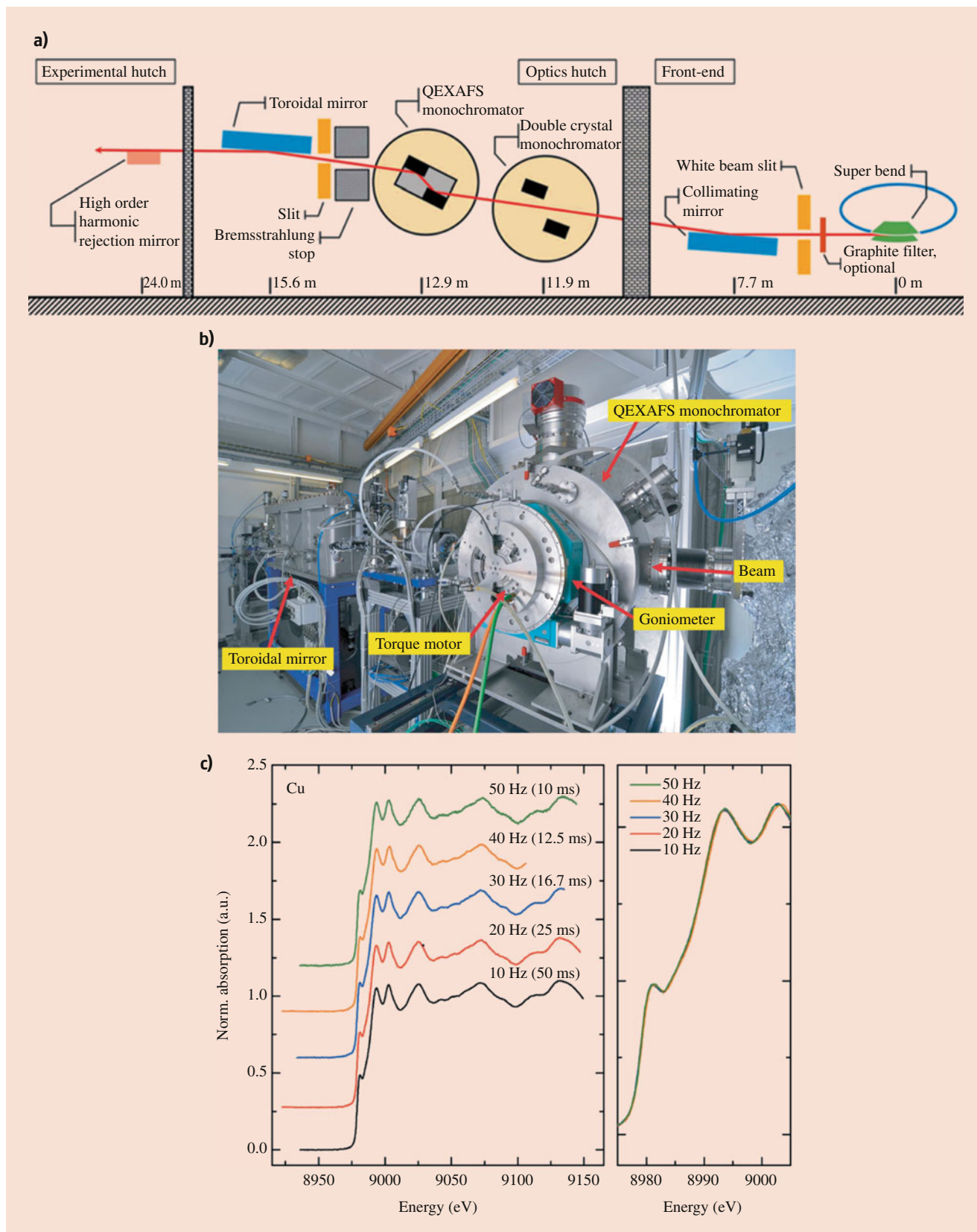
28.2.2 Spectral Versus Time Resolution

An important parameter for all spectroscopic experiments is resolution, which is defined as the capability of the used equipment to distinguish between different unit scales (e.g., time or length). Ideally, a measurement has both good spectral resolution (e.g., the amount of points that is measured between two wave numbers) so that one can identify and separate all important features in a spectrum, as well as a good time resolution so that you can conduct measurements quickly. Quick measurements allow the ability to maximize the amount of samples measured during your limited beamtime and/or to distinguish important transitions during a time-resolved experiment. However, spectral and time resolution are a weigh-off, as generally the first increases with increasing measurement time (either by a longer acquisition time or by increasing the amount of accumulations that make up one spectrum). Therefore, a balance needs to be found between the two, based on the aim of the experiment. Note that although advancement in equipment and methods plays an important part in optimizing the spectral resolution, time resolution is ultimately the limiting factor. With this in mind, it is important to realize that nowadays in XAS, the spectral resolution can be increased greatly without sacrificing time resolution. This is because of the implementation of energy-dispersive X-ray or QXAS equipment, both of which severely reduce the acquisition time (as well as the risk of sample damage) [21]. An example of a QXAS beamline is the X10DA at the Swiss Light Source (SLS) with a special monochromator developed by Wuppertal University, that can oscillate at several tens of Hz frequency, and is shown in Fig. 28.5. Just like spectral resolution, time resolution is largely determined by equipment, since machinery needs to move, detectors need to be read out, data needs to be saved,

etc. However, if we take these elements away, the factor that ultimately determines the maximum time resolution is the number of electrons (the bunches) in the storage ring. As mentioned earlier, light is generated in pulses in the GHz range, so for experiments with a timescale of seconds or longer, in all practicality, the X-ray light source can be deemed continuous. Still, the pulsed nature of the incoming X-ray radiation can be exploited to carry out transient experiments [2]. In the end, the time resolution of an experiment will be technically limited by the amount of electron bunches in the storage ring, the photon flux they generate (which differs per end-station/beamline type), the time required for mechanical movements of the equipment, and the readout speed of detectors and sensors. For more in-depth discussion of XAS theory, how synchrotrons work, and practical matters like how to prepare for X-ray spectroscopy experiments, we refer the reader to several excellent handbooks that are dedicated to XAS [1, 3, 4].

28.2.3 Spatially Resolved X-Ray Absorption Spectroscopy

An in-depth discussion of spatially resolved XAS methods is not within the scope of this chapter, but we feel any work on XAS in catalysis would be lacking if this possibility was not mentioned as more and more we are moving toward the spatiotemporal characterization of catalyst systems, i.e., simultaneously measuring the system as function of space and time and in essence taking snapshots of a catalysts at work. In short, there are several techniques that can combine imaging with time-resolved XAS that can be roughly divided into microscopy and computational techniques [22]. Not all spatially resolved techniques are suitable for all types of

Fig. 28.5 (**a**) Schematic overview of the X10DA beamline at the Swiss Light Source (SLS, Switzerland), one of the most advanced quick-X-ray absorption spectroscopy (QXAS) beamlines currently in operation, and which is used for the investigation of solid catalysts, including the example described in Fig. 28.9. (**b**) Photograph of the QEXAFS monochromator made by Wuppertal University, which enables the acquisition

in situ and *operando* measurements. Especially the computational measurements of "classic" heterogeneous catalysis processes with high spatial resolution are still very challenging. However, some beamlines are dedicated to the investigation of a niche form of catalysis, like the ATMOS beamline at the ALS for the investigation of batteries with X-ray ptychography or the BL36XU at SPring-8 for polymer electrolyte fuel cells (PEFCs) for computed tomography-XAS (CT-XAS) measurements [23]. For computed tomography techniques, the field of view and pixel sizes are (still) generally quite large for *operando* experiments (in the order of microns). Therefore, statistically relevant sampling sizes are generally obtained. However, for X-ray microscopy techniques, the obtained resolution is often much higher, and single particle approaches can be used, even under *in situ* and *operando* conditions. It is important to stress that one has to be aware that while X-ray microscopy can yield valuable insights, before drawing conclusions, statistically relevant amounts of samples or particles need to be analyzed. Conventional *operando* XAS is in principle a bulk technique and therefore does not generally suffer from this drawback. Using both soft and hard X-rays, several advances in *in situ* (and *ex situ*) spatially resolved X-ray microscopy have been published over the last decade. For example, using scanning transmission X-ray microscopy and soft X-rays, van Ravenhorst *et al.* were able to visually capture the genesis of an active Co/TiO_2 Fischer-Tropsch synthesis (FTS) catalyst particle using a MEMS reactor, shown in Fig. 28.4a, during a study lasting approximately 2 days. This study showed that during an induction period, the TiO_2 pores slowly fill with long-chain hydrocarbons, which takes several tens of hours and shows intraparticle hydrocarbon heterogeneities (Fig. 28.6) [24]. Such spatiotemporal differences in a single catalyst particle had previously not been brought to light and could only be captured by performing time-resolved long-duration *operando* XAS experiments. Cats *et al.* studied the same catalyst system with transmission X-ray microscopy (TXM) using hard X-rays, making use of the reactor cell shown in Fig. 28.4b. They were able to note similar intraparticle effects for Co as shown in the corresponding 2D TXM images (Fig. 28.7a). Furthermore, time-resolved long-duration XANES in 3D could be measured for an individual catalyst particle, and the study indicates that the catalyst material is under *operando* conditions mainly in its Co

metallic state. This X-ray microscopy technique has also shown to be particularly relevant for a fluid catalytic cracking (FCC) particle (shown in Fig. 28.7b, c) where 3D reconstructions with voxels of down to 20–30 nm showed detailed information of metal (i.e., Fe and Ni) speciation throughout the FCC particle (Meirer *et al.* [25]) as a function of reaction time, and more recently, a 3D reconstruction of the carbon speciation throughout the FCC catalyst particle (Vesely *et al.* [26]), allowing a detailed view of the flow resistance of the crude oil feedstock through the pore network, the ~50-µm-sized FCC particle in the absence and presence of metal deposits (i.e., a long-term catalyst deactivation phenomenon) and carbon deposits (i.e., a short-term catalyst deactivation phenomenon).

28.2.4 Choosing the Correct Experimental Mode

In order to choose the right mode of measurement (i.e., transmission or fluorescence), it is important to have a clear idea of the kind of information that should be contained in the acquired data. This includes the element of interest, more specifically its absorption edge energies, its concentration and distribution, and the physical state of the sample. Transmission experiments involve simply measuring the X-rays before and after passing through a sample (that should be uniform) in a straight line. Samples should not be too thick or too thin, with a rule of thumb of ~4 absorption lengths. Fluorescence mode can be employed either when the concentration of the element of interest is low in thick samples or high in thin samples. In fluorescence experiments not absorption but emission is detected, and the detector is placed at an angle. This angle is often chosen to be 90° of the incident beam, while the sample is placed at 45° to maximize emission yield and minimize noise from scattering. The sample angle can also be decreased to a grazing incidence-type setup. In this mode of measurement, the angle is chosen such that the penetration depth of the X-rays is limited to a few nanometers. This makes it possible to selectively investigate the surface of flat samples by detecting the X-ray fluorescence at 90°.

Fig. 28.5 (continued) of an X-ray absorption spectrum in the up and down movements of the monochromator with several tens of Hz frequency. (**c**) X-ray absorption spectra of the Cu K-edge recorded at different frequencies, 10, 20, … 50 Hz [65]. (Reproduced from [65], with permission from Wiley-VCH)
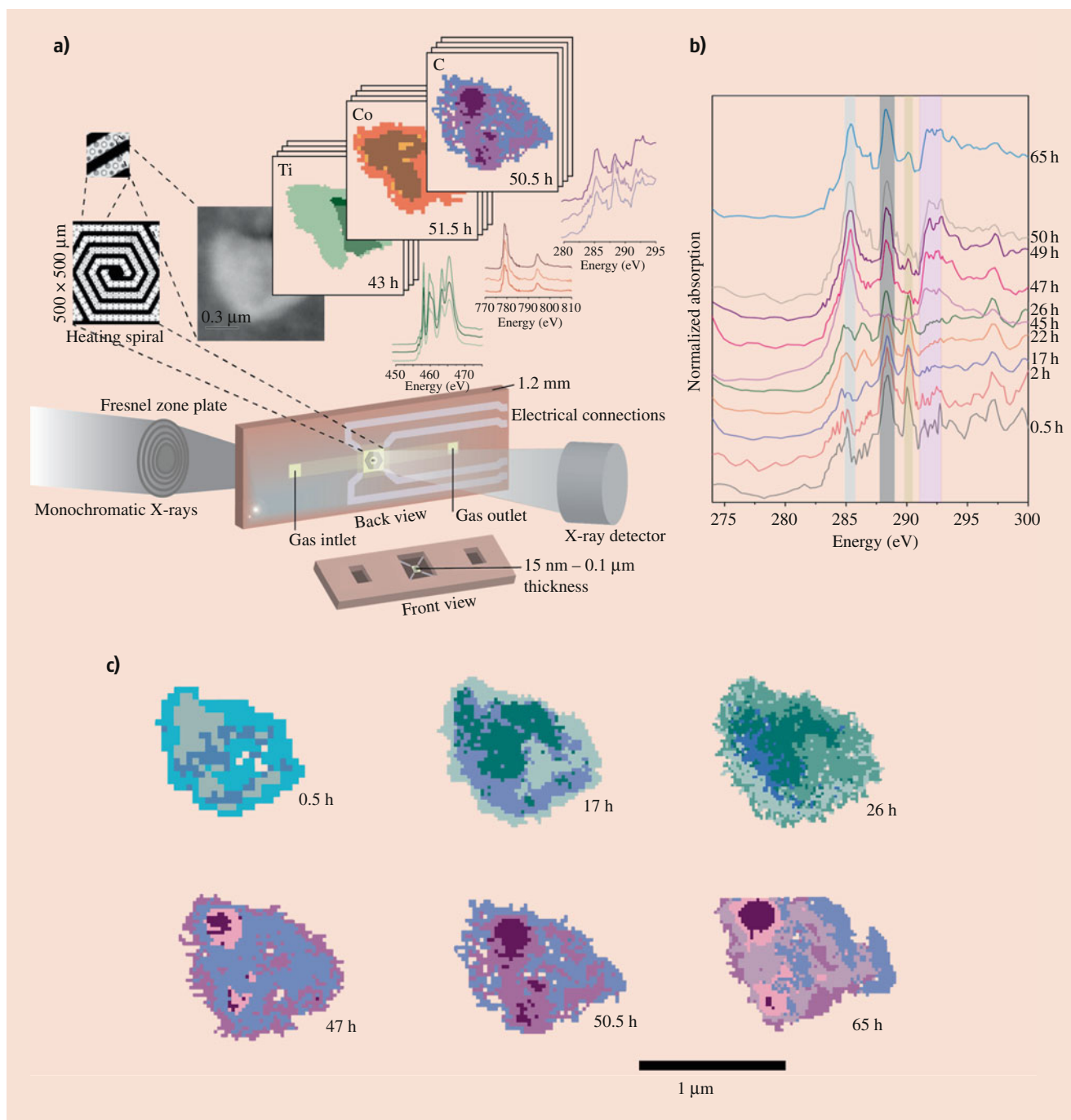
Fig. 28.6 Schematic overview of the *operando* micro-electromechanical system (MEMS) reactor and related data acquisition method by scanning transmission X-ray microscopy (STXM) for measuring a single Co/TiO₂ Fischer-Tropsch synthesis (FTS) catalyst particle as a function of both space and time. (**a**) Schematic representation of the MEMS reactor. Bottom-left, optical microscopy photograph of heating spiral with 0.1 μm overall thickness, with SiNₓ windows of 15 nm thickness containing the single Co/TiO₂ catalyst particles. Bottom, data acquisition method, the focused soft X-ray beam is changed in energy by the monochromator to measure an X-ray absorption spectrum for each pixel as a function of increasing time-on-stream [24]. (**b**) Time-resolved long-duration X-ray absorption spectra show the C-edge spectra of the catalyst particle, thereby capturing the organic part of an active Co/TiO₂ catalyst particle [56]. (**c**) Time-resolved long-duration spatial maps of an active Co/TiO₂ catalyst particle [56]. The different spectra represent different chemometrically resolved C-edge spectra, thereby gradually showing the different carbon species formed, including aromatic species, with increasing time-on-stream. (Reproduced with permission from [56])

Fig. 28.7 (**a**) Two time-resolved
long-duration 2D X-ray *operando*
nanotomography reconstructions
of a single Fischer-Tropsch
synthesis (FTS) Co/TiO₂ catalyst
particle [62]. The *in situ* X-ray
absorption near-edge
spectroscopy (XANES) data of
the cobalt K-edge are an example
of the data quality of K-edges
studied with this type of technique
and measured as a function of
reaction time. These results
indicate that cobalt mainly was
found in the metallic state under
FTS conditions with minor
contribution of CoTiO₃ [66]. (**b**)
3D X-ray nanotomography
reconstruction of a fluid catalytic
cracking (FCC) catalyst particle of
approximately 50 μm in diameter,
visualizing the distribution of Fe
and Ni in the FCC catalyst particle
as a function of its age (i.e., days).
(**c**) 3D X-ray nanotomography
reconstruction of an FCC catalyst
particle, with both Fe and Ni
distribution and the pore network
shown on its right-hand side the
pore network includes
streamlines, which illustrate the
connectivity between the different
macropores within the catalyst
particle [25]. The same system
was examined with X-ray
holotomography allowing the 3D
imaging of different carbon
deposits formed during the FCC
process. The carbon K-edge
spectra are shown to the right [26].
(Reproduced from [25, 62, 66],
with permission from Wiley-VCH
and AAAS)
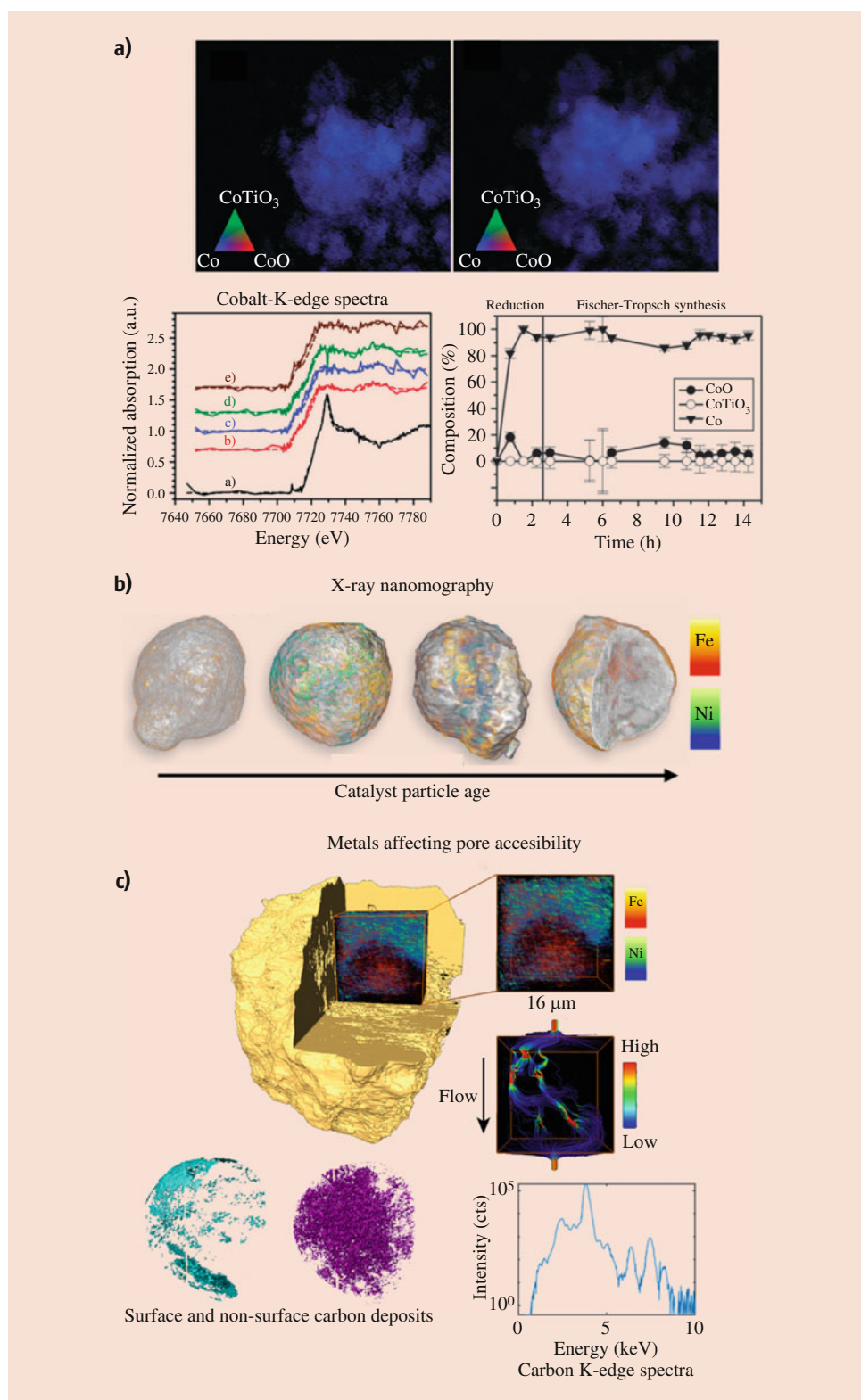
28.3 X-Ray Absorption Spectroscopy in Catalysis

In the previous section, we have described both qualitatively and quantitatively that synchrotron-based XAS is an extremely powerful characterization technique and capable of studying catalysts in a spatiotemporal manner. By selecting the proper incident energy, important characteristics of the material of interest can be studied, and even very small distortions in crystal structure can be detected. This not only holds for static samples but also for dynamic samples or systems when time resolution is high enough. XAS therefore enables the elucidation of how introduced species change the (average) state of the catalyst [27, 28]. This is exactly what we are interested in when we want to study catalysis. In catalysis research, important goals include the elucidation of active sites and (subsequent) structure-performance relationships [29]. For example, an in-depth understanding of reaction and deactivation mechanisms can lead to the design of new and improved catalytic processes in terms of activity, selectivity, stability, and as such can have major effects on sustainability and economic factors. Taking into account that 80% of all manufactured goods have encountered at least one catalyst in their production process [30], small improvements in such processes can be greatly advantageous both from an economical and a societal point of view.

In situ and *operando* spectroscopy offers the possibility to investigate various aspects of such catalytic processes in great detail as it is aimed at characterization of catalysts in their active state. Catalysts may also change their structure upon heating or when subjected to increased pressures, for example, metal nanoparticles are known to be dynamic in structure particularly at the elevated temperatures and pressures relevant to industrially applied catalysis [31–34]. Therefore, *ex situ* analysis will never be sufficiently capable of capturing the full complexity of a catalyst at work, and *in situ* or *operando* analysis is essential to generate relevant structure-performance relationships [35, 36]. The term *operando* spectroscopy is used when simultaneously analyzing reaction products made by the catalyst at work (usually by gas chromatography, GC, and/or mass spectrometry (MS)). More specifically, when using *operando* spectroscopy, one makes sure that the catalyst of interest is actually representative of the catalytic process aimed to study in terms of activity and (side) products. For example, *in situ* or *operando* UV-Vis spectroscopy can monitor the buildup of organics in a catalyst during reaction (e.g., polyaromatics or coke) [37], while *in situ* or *operando* infrared spectroscopy can provide a fingerprint-like molecular map of a reaction [38]. Such lab-based techniques are relatively easy to apply

even in *operando* mode – assuming a suitable reactor is available – but cannot always provide a complete picture. Sometimes, to unravel relevant important details of a (catalytic) process, information on the system is required that can only be obtained by using (advanced) X-ray-based characterization methods, for example, to yield highly specific and precise information on the local electronic environment of the catalyst materials (under reaction conditions) [39]. It is important to note that the design or use of a suitable *operando* reactor or cell is not trivial and requires serious consideration regarding your reaction, research goal, and the type of X-rays you will use [40]. Apart from the possibility to bring your own reactor, some beamlines also offer the possibility of using theirs [39, 41, 42].

As discussed above, XAS allows for the identification of parameters like coordination number, oxidation state, and local bond distances. Aside from these, the features in the spectra containing information on the different constituents all show up at different energies, both with regard to different elements as well as the different phases a specific element may boast in a sample. That means that XAS is element-specific (i.e., an element shows up in a XAS spectrum within a predetermined set range of energies) and that it can distinguish between different valences or coordination numbers of an element within this specific range of energies. This is especially useful for catalysis as a heterogeneous catalyst typically consists of an active material in the form of transition metal (oxide) nanoparticles[29] carried on a porous, metal oxide (e.g., SiO_2, Al_2O_3, and TiO_2) or carbonaceous support (e.g., active carbon and carbon nanofiber), most of which are materials suitable for (hard) X-ray *operando* studies [43] (recall that soft X-rays easily interact with light materials, which include gases, products, and even the *operando* cell, making *operando* soft X-ray studies more challenging). Therefore, in principle, the entire catalyst (i.e., both active material and support) can be characterized in depth, both in *ex situ* and *in situ/operando* modes. When introduced species, such as the aforementioned gaseous reactants, bind to the surface of the catalyst, corresponding changes in the average electronic structure can be observed in the spectra, and this information can be used to identify the oxidation state of the active phase. This holds true for many relevant processes like catalyst activation (e.g., reduction), catalytic conversion, and deactivation of the catalyst material. As such, after thorough analysis of the observed changes, a clear picture of the entire catalytic reaction can be obtained [44].

The events that a catalytic reaction encompasses take place simultaneously albeit on different timescales, ranging from picoseconds for bond breaking to (typically, depending

on the process) weeks-months-years for deactivation [34, 45–47]. The different timescales can all be investigated using XAS but require different approaches. For example, when trying to figure out the equilibrium state of the catalyst at work, often steady-state operation is used as the system then is most representative for industrial operation [46]. In principle, due to the equilibrium, the timescales involved are such that we do not need to sacrifice spectral resolution for time resolution. This is especially true due to the advent of QXAS. In contrast, when we want to investigate the exact moment a reactant first comes into contact with the catalyst, kinetics, or reaction intermediates, we want to look at shorter timescales which may also require different equipment or a different beamline altogether. Such alternate approaches may, for example, require introducing reactants in a pulsed fashion. It is important to realize that under such conditions, even when the reaction products are being monitored by GC/MS, the system is inherently not representative for its industrial counterpart (should there be one) even though such experiments are typically still referred to as *operando*.

Although technically you *could* measure steady-state or deactivation processes with sub-second or sub-microsecond resolution, the amount of data generated and that would require analysis would be very large (in the order of terabytes). If the scope is to learn more about deactivation, obtaining such an amount of data would not increase the chances of achieving your goal. Similarly, if you want to study a process taking place at a sub-second timescale, it would not make sense to use a time resolution of seconds or more since the information will be averaged out or not even recorded at all. Hence, a careful choice of the proper beamtime setup is important to realize the goals of a particular characterization study, including the type of catalysis (e.g., photocatalysis), and both short-duration and long-duration time-resolved studies have their merits to capture the transient behavior of catalysts under relevant reaction conditions.

28.4 Showcases from the Field of Heterogeneous Catalysis

### 28.4.1 Automotive Catalysis

Zeolites are an archetypal class of heterogeneous catalysts, combining shape selectivity originating from their ordered crystalline and microporous structure with catalytic activity originating from single sites, like Brønsted acid or metal ion sites. SSZ-13, a zeolite with the chabazite (CHA) topology meaning it consists of cages connected by 6- and 8-membered rings (Fig. 28.8a), is such a material, and its copper-exchanged derivative known as Cu-SSZ-13 has received a great deal of attention over its activity in selective

catalytic reduction (SCR) of NO_x with NH_3 as reducing agent. NH_3-SCR is currently already being applied in trucks and other vehicles that run on diesel. Cu-SSZ-13-catalyzed NH_3-SCR has been investigated intensively with numerous analytical methods, including time-resolved XAS. Figure 28.8 summarizes some important aspects of this catalytic process. First, in Fig. 28.8c, we see that this process involves two operational regimes: one at low temperature (standard), for example, when the engine is just being turned on, and one at high temperature (fast) [48, 49]. The distinct regimes favor different mechanisms [50–52] and therefore different reaction products. The different sites involved in catalysis comprise the different oxidation states (+1 and +2) Cu ions can adopt and where they are located within the zeolite framework (Fig. 28.8b), which can be identified using *operando* XAS. The (type of) species or sites these distinct Cu ions prefer to bind or coordinate to can be identified in the EXAFS, also revealing catalyst deactivation due to binding to poisons in the gas feed [53]. All these mechanisms were investigated with *operando* XAS on different timescales and conditions accommodating to the aim of the experiment.

The different temperature regimes for NH_3-SCR operation over zeolite Cu-SSZ-13 have been observed in time-resolved *operando* Cu K-edge XAS experiments at a number of different beamlines [49–52, 54]. During the low-temperature regime run at steady conversion, typically below 200 °C, lower NO conversion and N_2 production are observed in MS measurements compared to the high-temperature regime. Inspection of the XANES spectra at this low T shows both a pre-edge peak originating from Cu(II) (1s ➜ 3d) and an edge-rising peak attributed to Cu(I) (1s ➜ 4p). Comparison with reference spectra and application of linear combination fit (LCF) reveals that these species are present in around a 1:1 ratio, albeit that Cu(I) is only present as NH_3-solvated mobile species, whereas Cu(II) is present as both mobile NH_3-solvated species and framework-bound species. This distinction can also be observed in the k^2-weighted FT-EXAFS spectra, where part of the Cu(II) is observed as framework-coordinated species by an established, well-defined second shell peak in Fig. 28.8d. The other species predominantly show a first shell coordination number of 2 for Cu(I) and 4 for Cu(II) and induce perturbation in the second shell peak through their mobile nature (recall that more crystalline environments result in well-defined peaks, and vice versa). Upon moving to the high-T regime, these perturbations decrease through the formation of more framework-coordinated Cu (II) species, as is also observed in the XANES.

During the reaction in the low-T regime, XANES measurements revealed that the mobile Cu(II) species are reduced to Cu(I) by ammonia, before the latter species are oxidized back to Cu(II) to complete the redox cycle [50]. Transient *operando* XAS experiments in the form of LCF analysis of time-resolved QEXAFS spectra were conducted to track the

Fig. 28.8 Selective catalytic reduction (SCR) of NO$_x$ over Cu-loaded zeolite Cu-SSZ-13 catalysts. (**a**) Schematic of the chabazite (CHA) topology, which is the framework structure of the SSZ-13 zeolite; (**b**) zoom-in of the CHA framework showing the possible positions of the Cu ions in SSZ-13, namely, in the 8-membered ring (red) and the 6-membered ring (blue) [49, 51]; (**c**) the two typical NO$_x$ reduction reactions during SCR operation; (**d**) k^2-weighted extended X-ray absorption fine structure (EXAFS) spectra [54]; (**e**) *operando* X-ray absorption near-edge spectroscopy (XANES) spectra of Cu-SSZ-13 during low-temperature SCR of NO$_x$ under various conditions [67]; (**f**) *operando* XANES of the Cu-SSZ-13-catalyzed SCR recorded at various reaction temperatures [54]; (**g**) temperature-dependent evolution of Cu species related to NO conversion and NH$_3$ temperature-programmed desorption [52]. (Reproduced from [49, 51, 52, 54, 67], with permission from Wiley-VCH and Springer Nature Publications)
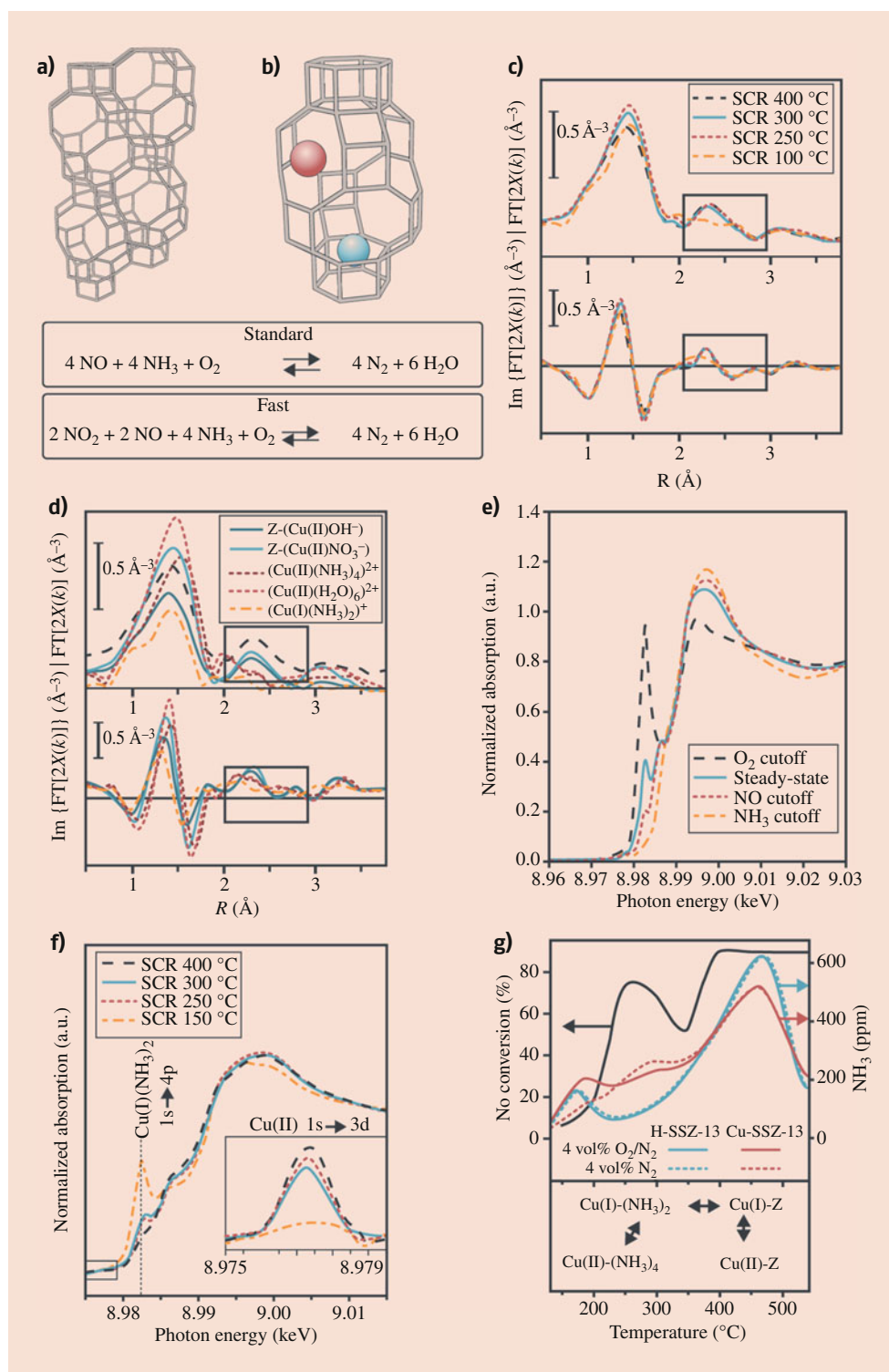
dynamic Cu speciation induced by the addition of NO to the gas feed. The results confirmed that in this operational regime, the reoxidation of twofold coordinated NH$_3$-solvated Cu(I) species to form the active fourfold coordinated Cu(II)-(NH$_3$)$_4$ species is the rate-limiting step of the reaction [52].

At temperatures above 350 °C, most Cu(II) is present as coordinated to zeolite framework, indicating a different mechanism is at play [48, 52].

In the high-temperature regime, Cu(I) species are still observed, even though Cu(II) species are postulated to be

the active site. The presence of stable Cu(I) species is therefore not desired, and insight into their continued presence is required in order to increase NH_3-SCR activity. Cu ions dispersed over and coordinated to well-defined materials like zeolites may seem similar activity-wise, but the fact is that the chemical environment in a 6- and in an 8-membered ring leads to differences in reducibility of Cu(II) in the presence of NH_3 [49]. Through fundamental alteration of the catalyst ensuring the presence of Cu ions only in 6-membered rings, *operando* XANES measurements revealed that the active Cu(II) species did not suffer from reduction into stable Cu(I) with subsequent loss of high-T regime SCR activity in this position. This indicates that merely Cu(II) present in 8-membered rings is sufficiently reducible to be converted into the stable Cu(I) under influence of NH_3 and high T.

Finally, catalyst deactivation can be caused by several factors, for instance, the presence of steam or impurities like SO_2 in the feedstock [53]. The first causes deactivation of zeolite-based materials by extracting Al from the framework, with a subsequent loss of Brønsted acid sites. However, as Ye et al. showed using XANES-based STXM, even when extra-framework Al species were generated upon treatment with steam, the Cu(II) sites proved to be very stable and remained active [55]. Whereas XANES shows that its presence can cause the formation of Cu bisulfate species which is detrimental for the activity of the catalyst, EXAFS also indicates that at low T the presence of SO_2 inhibits the formation of active sites. Such a combination of *operando* XAS studies of the different aspects of Cu-SSZ-13-catalyzed NH_3-SCR showcases that time-resolved XANES and EXAFS, especially when combined with other spectroscopic techniques, can provide fundamental understanding of the active sites, reaction mechanism, and deactivation of heterogeneous catalysts [49, 54].

28.4.2 Hydrogenation Catalysis

Heterogeneous catalysts often consist of metal nanoparticles supported on oxidic or carbonaceous material. The support materials can take on different crystal phases (e.g., titania can be present in the rutile, anatase, and brookite phase) or be amorphous. Porosity often varies throughout the support material, as large-scale preparation of such materials is not conducted with structure-inducing templates. Deposition of catalytic material on these supports is not always easy to control, leading to nanoparticles showing a size distribution and/or an inhomogeneous dispersion. Furthermore, metal nanoparticles are facetted, consequently supporting many kinds of sites available for interaction with reactants. The activity of certain sites can be enhanced by the addition of promotors or, oppositely, blocked to prevent deactivation or poisoning. Additionally, for many catalysts supported on

metal oxide supports, strong metal support interactions (SMSI) can take place. All of this complicates the analysis of such industrially relevant materials, especially under *operando* conditions where the catalyst material is in a dynamic state and changes continuously.

In conglomeration with (*operando*) characterization data from other analytical techniques and advanced data analysis, invaluable insights can be obtained on such systems through the use of time-resolved *operando* XAS. For instance, Vogt *et al.* studied Ni/SiO_2 catalysts with different particle sizes prepared by an industrial partner for CO_2 reduction with *operando* QXAS [38]. In their *operando* FT-IR spectra, they observed different reaction mechanisms occurring over the various Ni particle sizes, indicating structure sensitivity. They then conducted *operando* QXAS experiments probing the catalysts with alternating pulses of the reactant, CO_2, and a reducing gas, H_2. By recording spectra with a very high time resolution (100 ms), it was possible to study the dynamics of changes in nanoparticles at relevant timescales. Nevertheless, such experiments yielded enormous datasets (>70.000 spectra), and the authors set out to study very subtle changes (1–2% of absorption). To this end, the XANES spectra were analyzed by principal component analysis (PCA), which significantly reduced the noise level. Subsequent least square linear combination fitting with Ni and NiO references revealed subtle changes (1–2%) in oxidation state of the Ni catalysts as a result of the alternating pulses, as shown in Fig. 28.9. Among the different particle sizes, the subtle changes varied in accordance with FT-IR spectroscopy results that had shown the presence of different reaction mechanisms taking place depending on catalyst size. By relating these results, these/such distinct reaction pathways could be related to specific sites on the Ni nanoparticles, thus explaining the observed structure sensitivity. This study is an excellent example of high time resolution XAS and its relevance to millisecond dynamics of solid catalysts.

On the other hand, as mentioned before, catalytic processes have many relevant timescales. Recently, van Ravenhorst *et al.* published a time-resolved long-duration (i.e., 47 h) *operando* hard X-ray XAS study of Fischer-Tropsch synthesis (FTS) catalysis. A selection of the corresponding XANES data is shown in Fig. 28.10 [56]. Here the authors also used PCA and cluster analysis (CA) to reduce the 47 spectra into 5 clusters representing the largest variation in spectral changes. These five clusters happened to align chronologically, indicating a gradual change in the Co spectra during the FTS reaction which the authors linked to the formation of Co_2C, a commonly proposed deactivation mechanism. Interestingly, the formation of this cobalt carbide did not correlate to a decrease in activity, which does not support a common theory that the formation of Co_2C is linked to the deactivation mechanism of this catalyst material.
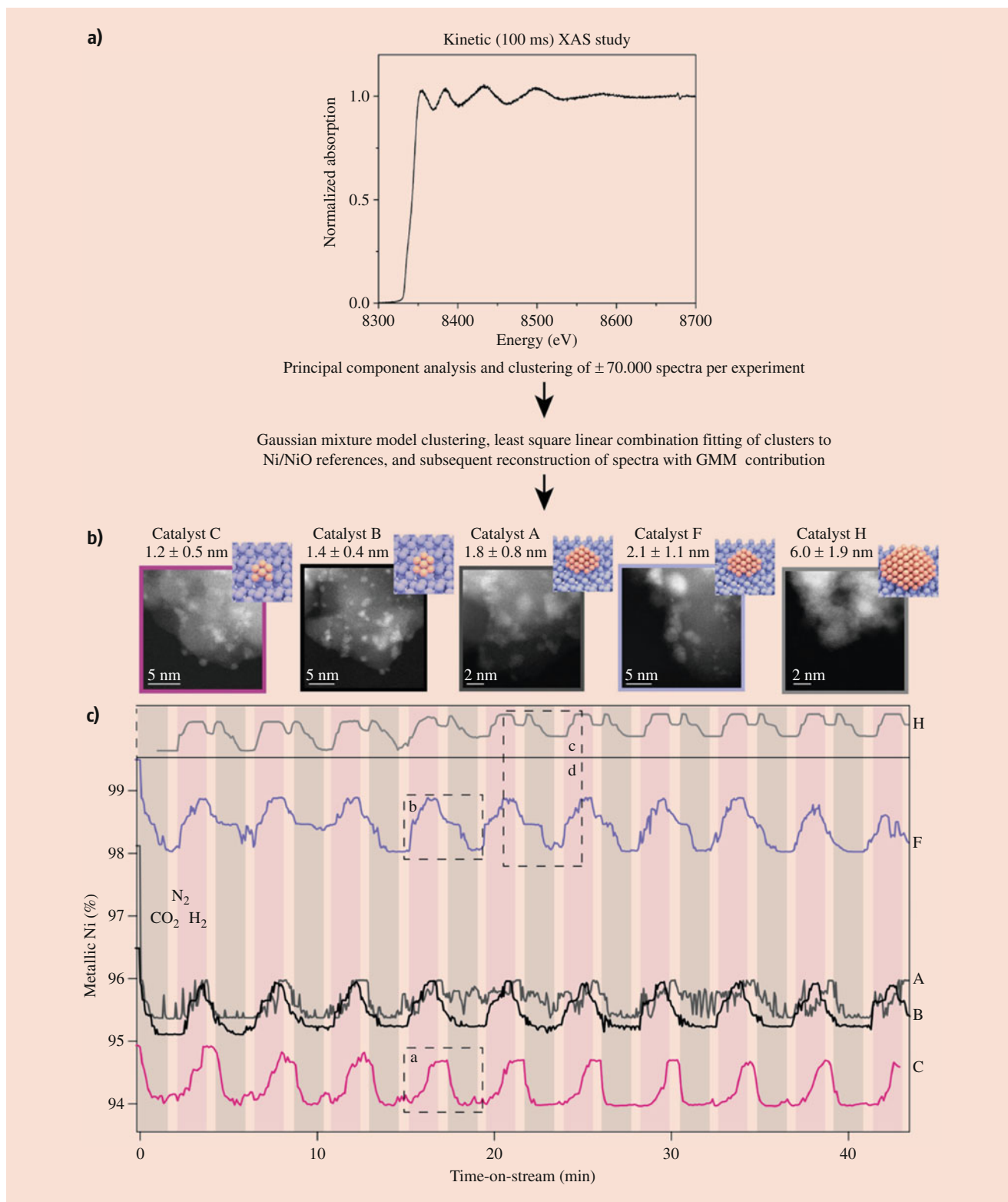
Fig. 28.9 A time-resolved short-duration *operando* X-ray absorption spectroscopy of a set of Ni/SiO$_2$ methanation catalysts. (**a**) Spectrum recorded at 100 ms time resolution in a study where kinetic details of the CO$_2$ methanation over Ni/SiO$_2$ catalyst materials with increasing Ni metal nanoparticle size were investigated [38]. (**b**) A selection of transmission electron microscopy (TEM) images of these catalyst. In several Ni/SiO$_2$ catalysts with differing mean particle size (1–6 nm), were studied with operando quick X-ray absorption spectroscopy (QXAS)

28.4.3 Electrocatalysis

Electrocatalytic processes are also a major point of interest for time-resolved XAS studies. Polymer electrolyte fuel cells (PEFCs) aimed at H_2 conversion for energy production, for instance, have been studied by a number of groups. The PEFCs often consist of a Pt catalyst supported on carbon as both the anode (H_2 dissociation) and the cathode (oxygen reduction reaction, ORR) catalyst. Especially the cathode side presents an interesting topic of study since the ORR over Pt catalysts suffers from slow kinetics and agglomeration of the Pt NPs that results in deactivation [57]. Due to dedicated *operando* PEFC setups representative for large-scale application that have been built at various beamlines, these materials are uniquely suited for advanced *operando* XAS studies. As such, the ORR over Pt/C under working conditions has been extensively investigated. For example, a study by the Tada group used time-resolved *operando* XAS to reveal oxidation kinetics at various potentials relevant for PEFC operation (i.e., 0.4–1.0 V) [58]. Additionally, they compared the pure Pt/C catalysts to bimetallic Pt_3Co/C catalysts. TEM and EXAFS confirmed that the latter consisted of an alloy Pt-Co core and a Pt-rich shell as the characteristics of Pt-Co bonding did not change upon oxidation, whereas the contribution of Pt-Pt decreased and a characteristic Pt-O shell was observed. Furthermore, they observed that upon alloying with Co (and Ni [59]), kinetic control of the Pt oxidation rate could be achieved. However, in a study involving accelerated degradation tests, they found that the long-term stability of Pt_3Co/C as cathode catalysts was not suitable for long-term successful PEFC operation [60]. This degradation was further investigated with computed tomography XAS, also denoted as CT-XAS. By rotating the sample 161° and recording XANES spectra at all angles, the catalyst could be reconstructed. Both Pt and Co were imaged, and this revealed differences between their degradation mechanisms that seemed to be largely influenced by cracks in the carbon support [61].

28.4.4 Photocatalysis

The field of photocatalysis is particularly interesting for time-resolved XAS studies with high resolutions, since photocatalytic processes occur on the sub-microsecond timescale.

For example, charge transfer processes taking place on the photocatalytically active metal center can be investigated using pump-probe techniques. This approach involves excitation of the catalyst under pulsed UV-Vis light typically in the order of ns, while the storage ring of the beamline operates in single or few bunches mode, resulting in X-ray pulses in the order of ps, separated (and limited) by the bunch frequency. Such an exploitation of the electron bunches when appropriately equilibrated with the probe can result in ns time resolution. This is demonstrated by Baran et al., who studied water splitting over a model α-Fe_2O_3/IrO_x catalyst using Ir-L_{III} XANES spectra, pulse-activated by 400 nm LED light in synchronization with the incoming X-rays. Comparison between illuminated and dark samples revealed that more holes were present in IrO_x during irradiation, inducing a cascade of charge transfers from the Fe_2O_3 layer to the IrO_x layer, resulting in more photo-generated holes. These holes in the IrO_x layer were observed through analyzing the density of states obtained from the XANES spectra, while the catalyst was operating under a realistic potential. A change in potential showed a change in the charge transfer process, whereby minor amounts of Ir(IV) were reduced to Ir(III), while transiently (in the order of ns) maintaining Ir(IV) coordination distances. In the XANES spectra, this resulted in a shift of the spectrum to lower energies [2]. Such a study showcases that time resolutions suitable for the detection of transient species, in this case 600 ns, can be achieved on catalysts when the capabilities of the equipment are properly exploited and the experiment is designed appropriately.

28.5 Toward Ultrafast X-Ray Spectroscopy of Catalysts

To push the time resolution down even further and into the direction of ps-fs, a different X-ray source can be employed, namely, FELs. This is demonstrated by the investigation of an elementary step in many heterogeneously catalyzed reactions: the dynamics of CO adsorption and desorption on metal surfaces in the absence and presence of, for example O_2. This exciting field of frontier research has been summarized in a recent article by Nilsson and co-workers [62]. A model Ru(0001) surface was employed, and CO was probed with soft X-rays to inspect the C-K-edge with XAS, and particularly the 1s ➜ π^* transition [63]. As CO adsorbs

◄

Fig. 28.9 (continued) by pulsing CO_2 and H_2, and comparing the QXAS data of the different particle size responses to those reactant pulses. The large amount of QXAS data recorded during each experiment was refined by several (multivariate) data analysis steps allowing the discrimination of several interesting particle-size-dependent phenomena of the CO_2 methanation reaction. (**c**) Differences between the different time-resolved metallic Ni contribution as a function of the pulse duration when switching between H_2 and CO_2. Inserts a and b as well as c and d show the dynamics of the Ni metal surface under different reaction environments and its dependency of the metal nanoparticle size. (Reproduced from [38], with permission from Nature Springer Publishers)
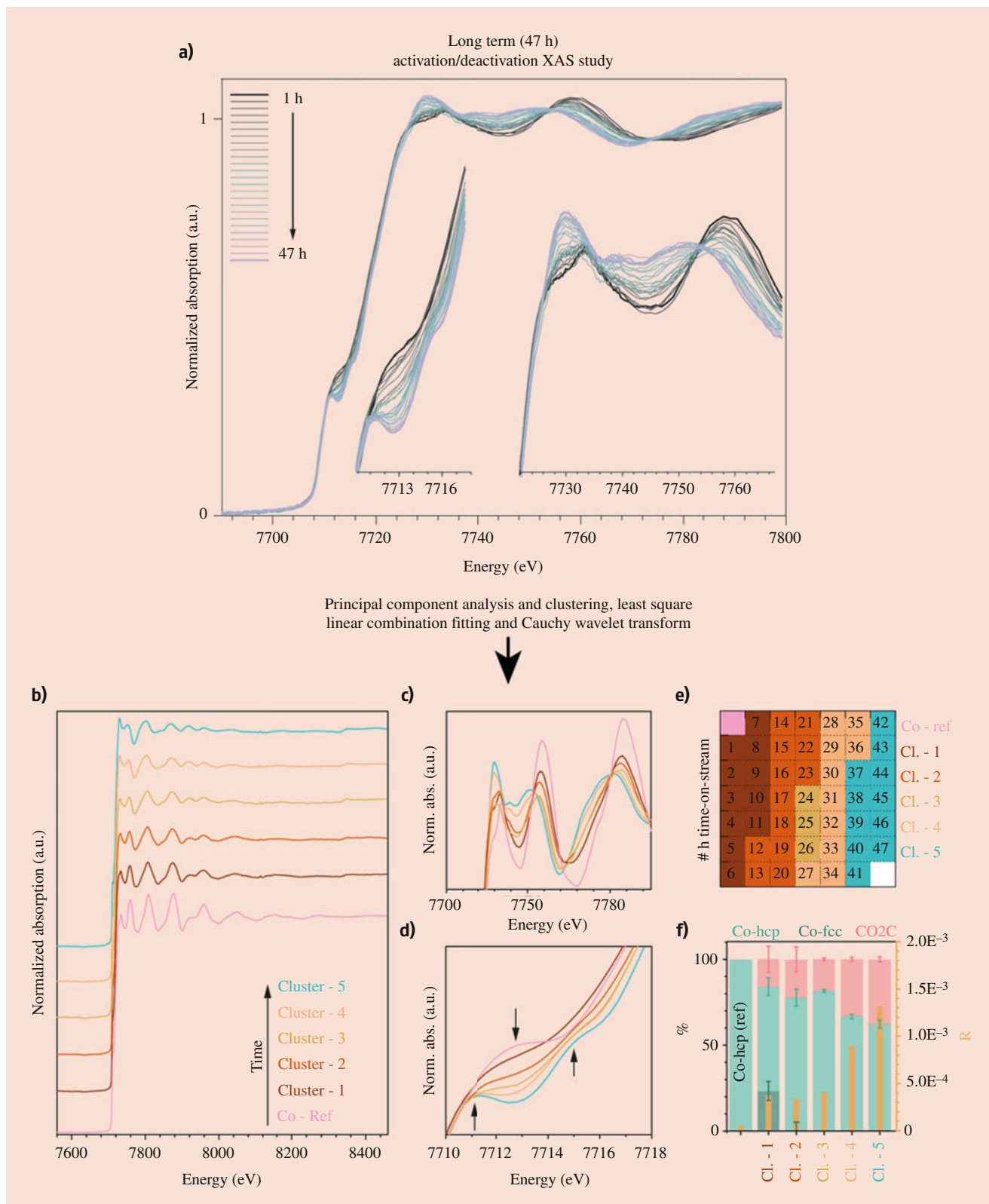
Fig. 28.10 (**a**) A time-resolved long-duration *operando* X-ray absorption spectroscopy study of a Co/TiO$_2$ Fischer-Tropsch synthesis (FTS) catalyst at 16 bar and 220 °C. (**b**) By performing principal component analysis (PCA) and cluster analysis (CA), the large number of X-ray absorption spectra obtained during 2 days of operation could be downsized to five different clusters representing the spectral changes observed, where the formation of cobalt carbide (a commonly proposed deactivation mechanism in FTS) could not be linked to a decrease in

linearly through the C atom, preferably on a top site, a change in this transition is indicative of a change in orientation of the CO molecule on the surface. Additionally, both in-plane and out-of-plane polarized beams were used to investigate the behavior of Ru(0001)-CO. Such changes in behavior of CO were brought about by pulsing the Ru(0001) surface with 400 nm light, heating it up. As such, XAS spectra revealed a redshift in the peak position upon of the surface. This redshift is attributed to an increase in population of the π* orbital. This indicates CO moving from a top to a bridge or hollow site, a phenomenon taking place on the ps timescale. In the ps that follow, the polarization-dependent XAS spectra show peaks closely resembling gas-phase CO, but still interacting with the surface in several configurations. Upon subsequent cooling down of the Ru(0001) substrate, only some CO desorbs completely, while most readsorbs to the surface. This indicates that the short-lived, transient phase is in fact a precursor state. The entire process described here takes place over a period of 25 ps, illustrating the potential of time-resolved XAS measurements conducted at FELs, an experimental approach which will become more frequently used in the upcoming decade.

28.6　Conclusions and Outlook

Time-resolved *in situ* and *operando* X-ray absorption spectroscopy (XAS) is a powerful analytical tool for heterogeneous catalysis research to shed new insights in their (local) structure and functioning, including their reaction and deactivation mechanism. XANES and EXAFS spectra allow in-depth characterization of solid catalysts under various conditions (hydrated, dehydrated, and reduced state) and, most importantly, in their working state (*operando* characterization approach) on different timescales, very short (milliseconds and faster) as well as very long (hours, days, and longer). Both timescales are of importance in the field of catalysis; especially the latter is sometimes forgotten as solid catalysts evolve toward their active state ("genesis" of the catalyst) and has to be evaluated as well during its deactivation phase to shed insight in deactivation phenomena in order to extend the lifetime of solid catalysts. The XAS methodology can be applied to a plethora of catalytic reactions ranging

from photocatalysis over electrocatalysis to thermocatalysis. Processes on different timescales can be investigated by smart exploitation of equipment and design of experiments. While a true *operando* experiment investigates the catalyst working at industrially relevant conditions in terms of gas feed composition, temperature, pressure, and reaction products formed, not all timescales relevant to catalysis can be investigated under the same conditions. Kinetics, intermediate species, and transient states are generally investigated on shorter timescales (ns-ps), using, for example, pulsed feed or excitation, lower conversion rates, or alternate catalyst compositions. Such measurements provide time-resolved XAS with the capability to investigate fundamental and short-lived phenomena occurring during catalytic reactions. However, as XAS is element-specific and can therefore only look at a single material at a time, it is important to combine time-resolved XAS with results from other spectroscopic and analytical methods, including theoretical modelling and chemometrics. Only through combing the insights obtained from a multi-technique characterization approach can we truly get to understand a catalytic process in depth.

In the coming decade, we expect that technological advancements in various fields will push down the time resolution for (Q)XAS even further without sacrificing spectral resolution or sample integrity. Next to that, we expect that developments in imaging methods, like *operando* X-ray microscopy and ptychography, will play a key role in revealing structure-performance relationships in all fields of catalysis with both high spatial and temporal resolution, especially combined with techniques from data science like unsupervised learning and data mining. It is expected that long-duration experiments at synchrotron radiation facilities, which can last for months or years, will become feasible by building setups which can be temporarily moved in and out of the X-ray beam, while still fully functional. Finally, the aforementioned technological advancements will not only play an important role at synchrotron radiation facilities and FELs, but they will also make lab-based XAS more viable as a standard laboratory technique, similar to lab-based [XRD] studies. This will make XAS so accessible that in the future we will be able to simply measure our XAS experiments whenever we want and under almost identical reaction conditions as we are currently doing in lab-based catalysis

Fig. 28.10 (continued) observed catalyst activity [56]. (**b, c**) A zoom-in of the areas with the highest amount of spectral changes. (**d**) The time frame of the different clusters with increasing time-on-stream. The colored boxes represent the cluster and the number represents the time in hours. The different clusters were fitted with the spectra of post-reduction, post-H$_2$ treatment (post-H$_2$) and the Co$_2$C reference, and the linear combination result with the residual is shown in (**e**). (**f**) With increasing time-on-stream, the amount of Co$_2$C phase increased, while the amount of metallic Co decreased. (Reproduced from [56], with permission from Wiley-VCH)

experiments, thereby allowing for time-resolved (e.g., an entire year or even longer) long-duration *operando* XAS measurements to fully capture the genesis, life, and death of a solid catalyst. In this manner, the *operando* concept can be fully captured as the experimental conditions of an industrial reactor can be best mimicked in a lab environment with the ultimate goal to make a molecular movie of the working catalyst.

References

1. Newton, M.A., Dent, A.J., Evans, J.: Bringing time resolution to EXAFS: recent developments and application to chemical systems. Chem. Soc. Rev. **31**, 83–95 (2002)
2. van Bokhoven, J., Lamberti, C. (eds.): X-Ray Absorption and X-Ray Emission Spectroscopy. Wiley, New York (2016)
3. Koningsberger, D.C., Prins, R. (eds.): X-Ray Absorption: Principles, Applications, Techniques of EXAFS, SEXAFS and XANES. Wiley, New York (1988)
4. Bordiga, S., Groppo, E., Agostini, G., Van Bokhoven, J.A., Lamberti, C.: Reactivity of surface species in heterogeneous catalysts probed by in situ X-ray absorption techniques. Chem. Rev. **113**, 1736–1850 (2013)
5. Iwasawa, Y., Asakura, K., Tada, M.: XAFS Techniques for Catalysts, Nanomaterials, and Surfaces. Springer, New York (2017)
6. Calvin, S.: XAFS for Everyone. CRC Press, Boca Raton (2013)
7. Bunker, G.: Introduction to XAFS. Cambridge University Press, Cambridge (2010)
8. Bearden, J.A., Burr, A.F.: Re-evaluation of X-ray atomic energy levels. Rev. Mod. Phys. **39**, 125–142 (1967)
9. Wong, J., Lytle, F.W., Messmer, R.P., Maylotte, D.H.: K-edge absorption spectra of selected vanadium compounds. Phys. Rev. B. **30**, 5596–5610 (1984)
10. Chen, L.X., et al.: X-ray snapshots for metalloporphyrin axial ligation. Chem. Sci. **1**, 642 (2010)
11. Chen, L.X., et al.: Tracking electrons and atoms in a Photoexcited Metalloporphyrin by X-ray transient absorption spectroscopy. J. Am. Chem. Soc. **129**, 9616–9618 (2007)
12. Sayers, D.E., Stern, E.A., Lytle, F.W.: New technique for investigating noncrystalline structures: Fourier analysis of the extended X-ray-absorption fine structure. Phys. Rev. Lett. **27**, 1204–1207 (1971)
13. Yano, J., Yachandra, V.K.: X-ray absorption spectroscopy. Photosynth. Res. **102**, 241–254 (2009)
14. (a) Meirer, F., Weckhuysen, B.M.: Spatial and temporal exploration of heterogeneous catalysts with synchrotron radiation. Nat. Rev. Mater. **3**, 324–340 (2018); (b) Beale, A.M., Jacques, S.D.M., Weckhuysen, B.M.: Chemical imaging of catalytic solids with synchrotron radiation. Chem. Soc. Rev. **39**, 4656–4672 (2010); (c) Beale, A.M., Jacques, S.D.M., Gibson, E.K., Di Michiel, M.:
Progress towards five dimensional diffraction imaging of functional materials under process conditions. *Coord. Chem. Rev.* **277**, 208–223 (2014); (d) Grunwaldt, J.D., Schroer, C.G.: Hard and soft X-ray microscopy and tomography in catalysis: Bridging the different time and length scales. *Chem. Soc. Rev.* **39**, 4741–4753 (2010)
15. Mobilio, S., Boscherini, F., Meneghini, C.: Synchrotron Radiation. Springer, Berlin (2015)
16. Moya-Cancino, J.G., et al.: Elucidating the K-edge X-ray absorption near-edge structure of cobalt carbide. ChemCatChem. **11**, 3042–3045 (2019)
17. Zimmermann, P., et al.: Modern X-ray spectroscopy: XAS and XES in the laboratory. Coord. Chem. Rev. **423**, 213466 (2020)
18. McNeil, B.W.J., Thompson, N.R.: X-ray free-electron lasers. Nat. Photonics. **4**, 814–821 (2010)
19. Dell'Angela, M., Parmigiani, F., Malvestuto, M.: Time resolved X-ray absorption spectroscopy in condensed matter: a road map to the future. J. Electron Spectros. Relat. Phenomena. **200**, 22–30 (2015)
20. Bressler, C., Chergui, M.: Ultrafast X-ray absorption spectroscopy. Chem. Rev. **104**, 1781–1812 (2004)
21. Prestipino, C., Mathon, O., Hino, R., Beteva, A., Pascarelli, S.: Quick-EXAFS implementation on the general purpose EXAFS beamline at ESRF. J. Synchrotron Radiat. **18**, 176–182 (2011)
22. Matsui, H., et al.: *Operando* XAFS imaging of distribution of Pt cathode catalysts in PEFC MEA. Chem. Rec. **19**, 1380–1392 (2019)
23. Uruga, T., et al.: SPring-8 BL36XU: synchrotron radiation X-ray-based multi-analytical beamline for polymer electrolyte fuel cells under operating conditions. Chem. Rec. **19**, 1444–1456 (2019)
24. van Ravenhorst, I.K., et al.: Capturing the genesis of an active Fischer–Tropsch synthesis catalyst with *operando* X-ray nanospectroscopy. Angew. Chem. Int. Ed. **57**, 11957–11962 (2018)
25. Meirer, F., et al.: Life and death of a single catalytic cracking particle. Sci. Adv. **1**, e1400199 (2015)
26. Vesely, A.M., et al.: 3-D X-ray nanotomography reveals different carbon deposition mechanisms in a single catalyst particle. ChemCatChem. **13**, 2494–2507 (2021)
27. Fabbri, E., Abbott, D.F., Nachtegaal, M., Schmidt, T.J.: *Operando* X-ray absorption spectroscopy: a powerful tool toward water splitting catalyst development. Curr. Opin. Electrochem. **5**, 20–26 (2017)
28. Bell, A.T.: The impact of nanoscience in heterogeneous catalysis. Science. **229**, 1688–1692 (2013)
29. Nørskov, J.K., et al.: The nature of the active site in heterogeneous metal catalysis. Chem. Soc. Rev. **37**, 2163–2171 (2008)
30. Hagen, J.: Industrial Catalysis: A Practical Approach. Wiley-VCH, Weinheim (2015)
31. Erlandsson, R.: Gas-induced restructuring of palladium model catalysts studied with atomic force microscopy. J. Vac. Sci. Technol. B Microelectron. Nanom. Struct. **9**, 825 (1991)
32. Gai, P.L.: Environmental high resolution electron microscopy of gas-catalyst reactions. Top. Catal. **8**, 97–113 (1999)
33. Rupprechter, G., Weilach, C.: Spectroscopic studies of surface-gas interactions and catalyst restructuring at ambient pressure: mind the gap! J. Phys. Condens. Matter. **20**, 184019 (2008)
34. Kalz, K.F., et al.: Future challenges in heterogeneous catalysis: understanding catalysts under dynamic reaction conditions. ChemCatChem. **9**, 17–29 (2017)
35. Weckhuysen, B.M.: Determining the active site in a catalytic process: *operando* spectroscopy is more than a buzzword. Phys. Chem. Chem. Phys. **5**, 4351–4360 (2003)
36. Bañares, M.A.: *Operando* spectroscopy: the knowledge bridge to assessing structure-performance relationships in catalyst nanoparticles. Adv. Mater. **23**, 5293–5301 (2011)
37. De Wispelaere, K., et al.: Insight into the effect of water on the methanol-to-olefins conversion in H-SAPO-34 from molecular simulations and *in situ* microspectroscopy. ACS Catal. **6**, 1991–2002 (2016)

38. Vogt, C., et al.: Unravelling structure sensitivity in CO_2 hydrogenation over nickel. Nat. Catal. **1**, 127–134 (2018)

39. Agostini, G., et al.: XAS/DRIFTS/MS spectroscopy for time-resolved *operando* investigations at high temperature. J. Synchrotron Radiat. **25**, 1745–1752 (2018)

40. Kondrat, S.A., van Bokhoven, J.A.: A perspective on counting catalytic active sites and rates of reaction using X-ray spectroscopy. Top. Catal. **62**, 1218–1227 (2018)

41. Bare, S.R., Boubnov, A., Hong, J., Hoffman, A.S.: The consortium for operando and advanced catalyst characterization via electronic spectroscopy and structure (Co-ACCESS) at Stanford synchrotron radiation lightsource (SSRL). Synchrotron Radiat. News. **33**, 15–19 (2020)

42. Marinkovic, N.S., Ehrlich, S.N., Northrup, P., Chu, Y., Frenkel, A.I.: Synchrotron catalysis consortium (SCC) at NSLS-II: dedicated beamline facilities for *in situ* and *operando* characterization of catalysts. Synchrotron Radiat. News. **33**, 4–9 (2020)

43. Frenkel, A.I., Hills, C.W., Nuzzo, R.G.: A view from the inside: complexity in the atomic scale ordering of supported metal nanoparticles. J. Phys. Chem. B. **105**, 12689–12703 (2001)

44. Timoshenko, J., Roldan Cuenya, B.: *In situ/operando* electrocatalyst characterization by X-ray absorption spectroscopy. Chem. Rev. **121**, 882–961 (2020)

45. Rothenberg, G.: Catalysis: Concepts and Green Applications. Wiley-VCH, Weinheim (2017)

46. Chorkendorff, I., Niemantsverdriet, J.W.: Concepts of Modern Catalysis and Kinetics, 3rd edn. Wiley-VCH, Weinheim (2013)

47. Calderone, V.R., et al.: De Novo Design of Nanostructured Iron-Cobalt Fischer-Tropsch Catalysts. Angew. Chem. Int. Ed. **52**, 4397–4401 (2013)

48. Krishna, S.H., Jones, C.B., Miller, J.T., Ribeiro, F.H., Gounder, R.: Combining kinetics and operando spectroscopy to interrogate the mechanism and active site requirements of NO_x selective catalytic reduction with NH_3 on Cu-zeolites. J. Phys. Chem. Lett. **11**, 5029–5036 (2020)

49. Greenaway, A.G., et al.: *Operando* spectroscopic studies of Cu–SSZ-13 for NH_3–SCR deNO$_x$ investigates the role of NH_3 in observed Cu(II) reduction at high NO conversions. Top. Catal. **61**, 175–182 (2018)

50. Liu, C., et al.: *In situ* spectroscopic studies on the redox cycle of NH_3−SCR over Cu−CHA zeolites. ChemCatChem. **12**, 3050–3059 (2020)

51. Paolucci, C., et al.: Dynamic multinuclear sites formed by mobilized copper ions in NO_x by selective catalytic reduction. Science. **357**, 898–903 (2017)

52. Marberger, A., et al.: Time-resolved copper speciation during selective catalytic reduction of NO on Cu-SSZ-13. Nat. Catal. **1**, 221–227 (2018)

53. Bergman, S.L., et al.: *In-situ* studies of oxidation/reduction of copper in Cu-CHA SCR catalysts: comparison of fresh and SO_2-poisoned catalysts. Appl. Catal. B Environ. **269**, 118722 (2020)

54. Lomachenko, K.A., et al.: The Cu-CHA deNO$_x$ catalyst in action: temperature-dependent NH_3-assisted selective catalytic reduction monitored by operando XAS and XES. J. Am. Chem. Soc. **138**, 12025–12028 (2016)

55. Ye, X., et al.: Deactivation of Cu-exchanged automotive-emission NH_3-SCR catalysts elucidated with nanoscale resolution using scanning transmission X-ray microscopy. Angew. Chem. Int. Ed. **59**, 15610–15617 (2020)

56. van Ravenhorst, I.K., et al.: On the cobalt carbide formation in a Co/TiO_2 Fischer-Tropsch synthesis catalyst as studied by high-pressure, long-term operando X-ray absorption and diffraction. ACS Catal. **11**, 2956–2967 (2021)

57. Karan, K.: PEFC catalyst layer: recent advances in materials, microstructural characterization, and modeling. Curr. Opin. Electrochem. **5**, 27–35 (2017)

58. Ozawa, S., et al.: *Operando* time-resolved X-ray absorption fine structure study for Pt oxidation kinetics on Pt/C and Pt$_3$Co/C cathode catalysts by polymer electrolyte fuel cell voltage operation synchronized with rapid O_2 exposure. J. Phys. Chem. C. **122**, 14511–14517 (2018)

59. Ishiguro, N., et al.: Rate enhancements in structural transformations of Pt-Co and Pt-Ni bimetallic cathode catalysts in polymer electrolyte fuel cells studied by *in situ* time-resolved X-ray absorption fine structure. J. Phys. Chem. C. **118**, 15874–15883 (2014)

60. Tan, Y., Matsui, H., Ishiguro, N., Tada, M.: Three-dimensional XAFS imaging of polymer electrolyte fuel cell cathode catalysts in membrane electrode assembly. Acc. Mater. Surf. Res. **3**, 165–171 (2018)

61. Tan, Y., et al.: Pt-Co/C cathode catalyst degradation in a polymer electrolyte fuel cell investigated by an infographic approach combining three-dimensional spectro-imaging and unsupervised learning. J. Phys. Chem. C. **123**, 18844–18853 (2019)

62. Nilsson, A., et al.: Catalysis in real time using X-ray lasers. Chem. Phys. Lett. **675**, 145–173 (2017)

63. Wang, H.Y., et al.: Time-resolved observation of transient precursor state of CO on Ru(0001) using carbon K-edge spectroscopy. Phys. Chem. Chem. Phys. **22**, 2677–2684 (2020)

64. Moya-Cancino, J.G., et al.: *In-situ* X-ray absorption near edge structure spectroscopy of a solid catalyst using a laboratory-based set-up. ChemCatChem. **11**, 1039–1044 (2019)

65. Müller, O.: Hard X-Ray Synchrotron Beamline Instrumentation for Millisecond Quick Extended X-Ray Absorption Spectroscopy. Universitätsbibliothek Wuppertal (2016)

66. Cats, K.H., et al.: X-ray nanoscopy of cobalt Fischer-Tropsch catalysts at work. Chem. Commun. **49**, 4622–4624 (2013)

67. Paolucci, C., et al.: Isolation of the copper redox steps in the standard selective catalytic reduction on Cu-SSZ-13. Angew. Chem. Int. Ed. **53**, 11828–11833 (2014)

Bert M. Weckhuysen is Distinguished University Professor at Utrecht University. His group focuses on the development of *in situ* and *operando* spectroscopy and microscopy to investigate solid catalysts at work. For his work, he has received national and international awards, including the International Catalysis Award and the Spinoza Prize. He is an elected (foreign) member of a.o. KNAW, KVAB, and Academia Europaea.

Caterina Suzanna Wondergem received her PhD from Utrecht University, the Netherlands, in 2019. During this time, she worked on the development of *in situ* techniques for heterogeneous catalysis with professor Bert Weckhuysen. In 2020, she received a JSPS postdoctoral fellowship from the Japanese Society for the Promotion of Science to work on advanced X-ray imaging of electrocatalysts at Nagoya University, and in 2021 was promoted to designated assistant professor at the same institute.

Charlotte Vogt received her PhD with highest distinctions from Utrecht University in 2020 working with professor Bert Weckhuysen. In 2021, she was named one of "Forbes 30 under 30 Europe" and started her own research group as assistant professor at the Technion Institute for Technology in Israel, which focuses on a deep fundamental understanding of catalytic processes.